OPEN ACCESS

TRANSLATIONAL SCIENCE

# TNF is a homoeostatic regulator of distinct epigenetically primed human osteoclast precursors

Cecilia Ansalone, John Cole, Sabarinadh Chilaka, Flavia Sunzini, Shatakshi Sood, Jamie Robertson, Stefan Siebert, Iain B McInnes, Carl S Goodyear

**Handling editor** Josef S Smolen

► Additional material is published online only. To view, please visit the journal online (http://dx.doi.org/10.1136/annrheumdis-2020-219262).

Institute of Infection, Immunity and Inflammation, University of Glasgow, Glasgow, UK

**Correspondence to**
Professor Carl S Goodyear, Institute of Infection, Immunity and Inflammation, University of Glasgow, Glasgow G12 8TA, UK;
carl.goodyear@glasgow.ac.uk

Part of this study was previously presented at the 2017 ACR/ARHP Annual Meeting, Arthritis Rheumatol. 2017; 69 (suppl 10).

Received 8 October 2020
Revised 31 December 2020
Accepted 25 January 2021
Published Online First 10 March 2021



**To cite:** Ansalone C, Cole J, Chilaka S, *et al*. *Ann Rheum Dis* 2021;**80**:748–757.

## ABSTRACT

**Objectives** Circulating myeloid precursors are responsible for post-natal osteoclast (OC) differentiation and skeletal health, although the exact human precursors have not been defined. Enhanced osteoclastogenesis contributes to joint destruction in rheumatoid arthritis (RA) and tumour necrosis factor (TNF) is a well-known pro-osteoclastogenic factor. Herein, we investigated the interplay between receptor activator of nuclear factor kappa-B ligand (RANK-L), indispensable for fusion of myeloid precursors and the normal development of OCs, and TNF in directing the differentiation of diverse pre-OC populations derived from human peripheral blood.

**Methods** Flow cytometric cell sorting and analysis was used to assess the potential of myeloid populations to differentiate into OCs. Transcriptomic, epigenetic analysis, receptor expression and inhibitor experiments were used to unravel RANK-L and TNF signalling hierarchy.

**Results** TNF can act as a critical homoeostatic regulator of $CD14^+$ monocyte (MO) differentiation into OCs by inhibiting osteoclastogenesis to favour macrophage development. In contrast, a distinct previously unidentified $CD14^-CD16^-CD11c^+$ myeloid pre-OC population was exempt from this negative regulation. In healthy $CD14^+$ MOs, TNF drove epigenetic modification of the RANK promoter via a TNFR1-IKKβ-dependent pathway and halted osteoclastogenesis. In a subset of patients with RA, $CD14^+$ MOs exhibited an altered epigenetic state that resulted in dysregulated TNF-mediated OC homoeostasis.

**Conclusions** These findings fundamentally re-define the relationship between RANK-L and TNF. Moreover, they have identified a novel pool of human circulating non-MO OC precursors that unlike MOs are epigenetically preconditioned to ignore TNF-mediated signalling. In RA, this epigenetic preconditioning occurs in the MO compartment providing a pathological consequence of failure of this pathway.

### Key message

**What is already known about this subject?**

- OC differentiation and maturation from myeloid precursors relies on receptor activator of nuclear factor kappa-B (RANK) signalling and murine studies suggest that tumour necrosis factor (TNF) is a potent coactivator.
- One of the gold standard therapy for rheumatoid arthritis includes blocking TNF although a consistent portion of patients do not respond and display progressive joint destruction.

**What does this study add?**

- We have discovered a novel non-monocyte (MO) osteoclast (OC) precursor population in the human peripheral blood and demonstrated its epigenetic and transcriptomic imprint towards OC differentiation.
- We have demonstrated that TNF can act as a homoeostatic regulator of classical peripheral $CD14^+$ MOs by inhibiting their differentiation into OCs to favour macrophages and showed how this mechanism is epigenetically perturbated in a portion of patients with rheumatoid arthritis (RA) with active disease.

**How might this impact on clinical practice or future developments?**

- These data provide an important insight into the cellular and epigenetic heterogeneity in RA and can be used to develop alternative therapeutics for those patients that do not respond to current therapies.

## INTRODUCTION

Osteoclasts (OCs) are polykarion bone-resorbing cells that can be derived from either yolk sac erythro-myeloid progenitors or bone marrow/circulating monocyte (MO) precursors[1] supported by the receptor activator of nuclear factor kappa-B (RANK) receptor and tumour necrosis factor (TNF) family cytokine RANK-ligand (RANK-L).[2 3] Circulating MO also have the capacity to differentiate into macrophages (Mφ) or dendritic cells (DCs).[4 5] Recently, human ontogenetic and transcriptomic studies have re-classified DCs, MO, MO-derived cells and tissue resident Mφ based on their differentiation from specific precursor cells.[6 7] While murine studies have identified specific OC myeloid precursors[8] that play a crucial role in post-natal OC differentiation in vivo,[1], it is unclear whether specific non-MO circulating OC precursors exist in humans. Moreover, how such precursors respond to competing differentiating and activating cytokine signals and select their eventual cell fate is poorly understood.

Murine studies have shown that in combination with RANK-L, TNF is a direct maturation/activation stimulus of OC precursors.[9–11] It has been assumed that TNF mediates equivalent actions across human OC precursors. Consistent with this notion, TNF is one of the main mediators of joint inflammation in inflammatory diseases such

as rheumatoid arthritis (RA), which is associated with articular damage and systemic bone loss.[12 13] Furthermore, in the clinical setting, treatment with TNF inhibitors has been shown to reduce articular erosion.[14] However, the precise effects of TNF acting directly on human myeloid/MO/OC precursors remains ill-defined. Inflamed tissues, both in acute or chronic states, exhibit elevated levels of TNF, usually associated with MO recruitment and maturation even in the presence of RANK-L.[15] It is unclear why in environments that are favourable to osteoclastogenesis, a preponderance of infiltrating myeloid precursors does not differentiate down the OC lineage.

Herein, we report the existence of a human $CD14^-CD16^-CD11c^+$ myeloid precursor population that is epigenetically predisposed to rapidly differentiate into OCs. Notably, this population is unresponsive to a previously unrecognised homoeostatic TNF-mediated signal that fundamentally governs cell fate decisions in $CD14^+$ MOs that favours Mφ development. Moreover, we provide evidence that this effect is mediated by TNF via epigenetic regulation of the RANK promoter in circulating $CD14^+$ MOs and that this pathway is perturbed in RA.

## MATERIALS AND METHODS

Detailed experimental procedures and analyses are provided in online supplemental files.

## RESULTS

### Distinct epigenetically primed OC precursors in human blood

Circulating $CD14^+$ MOs are regarded as classical OC precursors,[16] but the existence of a distinct circulating human precursor is not known. To investigate the osteoclastogenic potential of circulating human myeloid cells we used fluorescence-activated cell sorting (figure 1A) to purify circulating MO subsets (classical $Lin^-HLA^-DR^+CD14^+CD16^-$, intermediate $Lin^-HLA^-DR^+CD14^+CD16^+$ and non-classical $Lin^-HLA^-DR^+CD14^{dim}CD16^{++}$) and other myeloid cells ($Lin^-HLA^-DR^+CD14^-CD16^-$). Culture of these populations with macrophage-colony stimulating factor (M-CSF) and RANK-L verified that classical MOs differentiate into mature OCs while intermediate and non-classical populations only produced few and variable numbers of small OCs[17] (figure 1B,C). Intriguingly, purified $Lin^-HLA^-DR^+CD14^-CD16^-$ myeloid cells differentiated into OCs, with numbers comparable to classical $CD14^+$ MOs (figure 1B,C). $Lin^-HLA^-DR^+CD14^-CD16^-$ myeloid cells can be subdivided via CD11c expression into populations that contain conventional pre-DCs ($CD14^-CD16^-CD11c^+$) and plasmacytoid DCs ($CD14^-CD16^-CD11c^-$)[7]; only the $CD14^-CD16^-CD11c^+$ population was able to adhere and differentiate into mature OCs (figure 1D).

The in vivo kinetics of osteoclastogenesis from precursors to a mature OC are not clear in humans, however, murine studies have shown that preconditioned cells can mature into OCs within 48 hours.[18] The in vitro generation of a mature OCs from circulating $CD14^+$ MOs or in vitro differentiated MO-derived pre/immature DCs or Mφ takes in excess of 7–14 days.[5 19 20] We hypothesised that this reflects the non-preconditioned state of the precursor and thus time is required for in vitro cell differentiation/trans-differentiation. In support of this, $CD14^+$ MOs are preincubated overnight with M-CSF to generate $CD14^+$ pre-OCs. This preincubation leads to upregulation of RANK and CSF1R (M-CSF receptor) transcripts (figure 1E),[21] and increased tri-methylation of histone H3 at lysine 4 (H3K4me3) in the RANK promoter (figure 1E), indicative of a transcriptionally active epigenetic state.[22] In comparison, immediate ex vivo evaluation of the identified $CD14^-CD16^-CD11c^+$ myeloid population revealed that they have higher levels of RANK transcript and decreased levels of CSF1R compared with classical $CD14^+$ MOs (figure 1F). This was associated with an increased level of H3K4me3 at the RANK promoter but less at the CSF1R promoter of $CD14^-CD16^-CD11c^+$ myeloid population compared with donor-matched $CD14^+$ MOs (figure 1F). Pre-OCs from both $CD14^+$ MOs and $CD14^-CD16^-CD11c^+$ cells were generated by M-CSF overnight incubation. Assessment of OC differentiation 72 hours post-RANK-L stimulation, revealed that while $CD14^+$ pre-OCs produce few small OCs at this time point, $CD11c^+$ pre-OCs rapidly differentiate into macroscopically larger OCs, with numbers significantly higher than those differentiated from donor-matched $CD14^+$ pre-OCs (figure 1G). Taken together, these results suggest that the circulating $CD14^-CD16^-CD11c^+$ myeloid population contains OC precursors that are in an epigenetically precommitted state to rapidly differentiate into mature OCs.

### TNF over-rides RANKL-driven osteoclastogenesis of $CD14^+$ circulating precursors but not $CD14^-CD16^-CD11c^+$ precursors

TNF is a well-known pro-osteoclastogenic factor, both in vitro[9 10 23] and in vivo.[24–26] However, nothing is known about how human circulating precursors respond to simultaneous exposure to TNF family member cytokines, as would be expected in a physiological setting. Therefore, we simultaneously stimulated human $CD14^+$ pre-OCs and $CD11c^+$ pre-OCs with RANK-L and TNF. Unexpectedly, we found that synchronised stimulation of $CD14^+$ pre-OCs with RANK-L and TNF resulted in substantial inhibition of osteoclastogenesis (figure 2A,B). The resulting cells exhibited Mφ morphology, although dissimilar to either regulatory M-CSF-driven Mφ (M-Mφ) or pro-inflammatory GM-CSF-driven Mφ (GM-Mφ) (online supplemental figure S1).

In comparison to what was observed in $CD14^+$ pre-OCs, TNF was unable to inhibit the generation of mature OCs derived from $CD11c^+$ pre-OCs (figure 2A,B). Extending the duration of differentiation to 14 days, we found that TNF completely abrogated the resorptive activity of $CD14^+$ pre-OCs but had no effect on $CD11c^+$ pre-OCs resorption (figure 2C,D). In order to demonstrate that $CD11c^+$ pre-OCs were not completely unresponsive to TNF, the secretion of relevant cytokines was evaluated. Notably, TNF stimulation resulted in the increased secretion of interferon-γ in $CD11c^+$ pre-OCs but not $CD14^+$ pre-OCs (online supplemental figure S2). Conversely, TNF stimulation resulted in the secretion of interleukin (IL)-12, IL-1β and IL-6 in $CD14^+$ pre-OCs but not $CD11c^+$ pre-OCs (online supplemental figure S2). Thus, circulating $CD14^-CD16^-CD11c^+$ precursors and $CD14^+$ MOs display a fundamental difference in their response to TNF, with $CD14^-CD16^-CD11c^+$ precursors able to differentiate into mature and functional OCs.

### TNF-mediated epigenetic modification of the RANK promoter controls RANK transcription and expression in $CD14^+$-derived OC precursors

To further explore the unexpected inhibition of osteoclastogenesis by TNF, we extended our cellular and molecular characterisation of $CD14^+$ pre-OCs. Increasing RANK-L concentration to potentially outcompete the simultaneous TNF signal did not restore OC differentiation (figure 3A). In comparison, there was a TNF dose-dependent reduction in the development of mature multinucleated OCs (figure 3B). To demonstrate TNF specificity and exclude the possibility of cross-contamination, addition

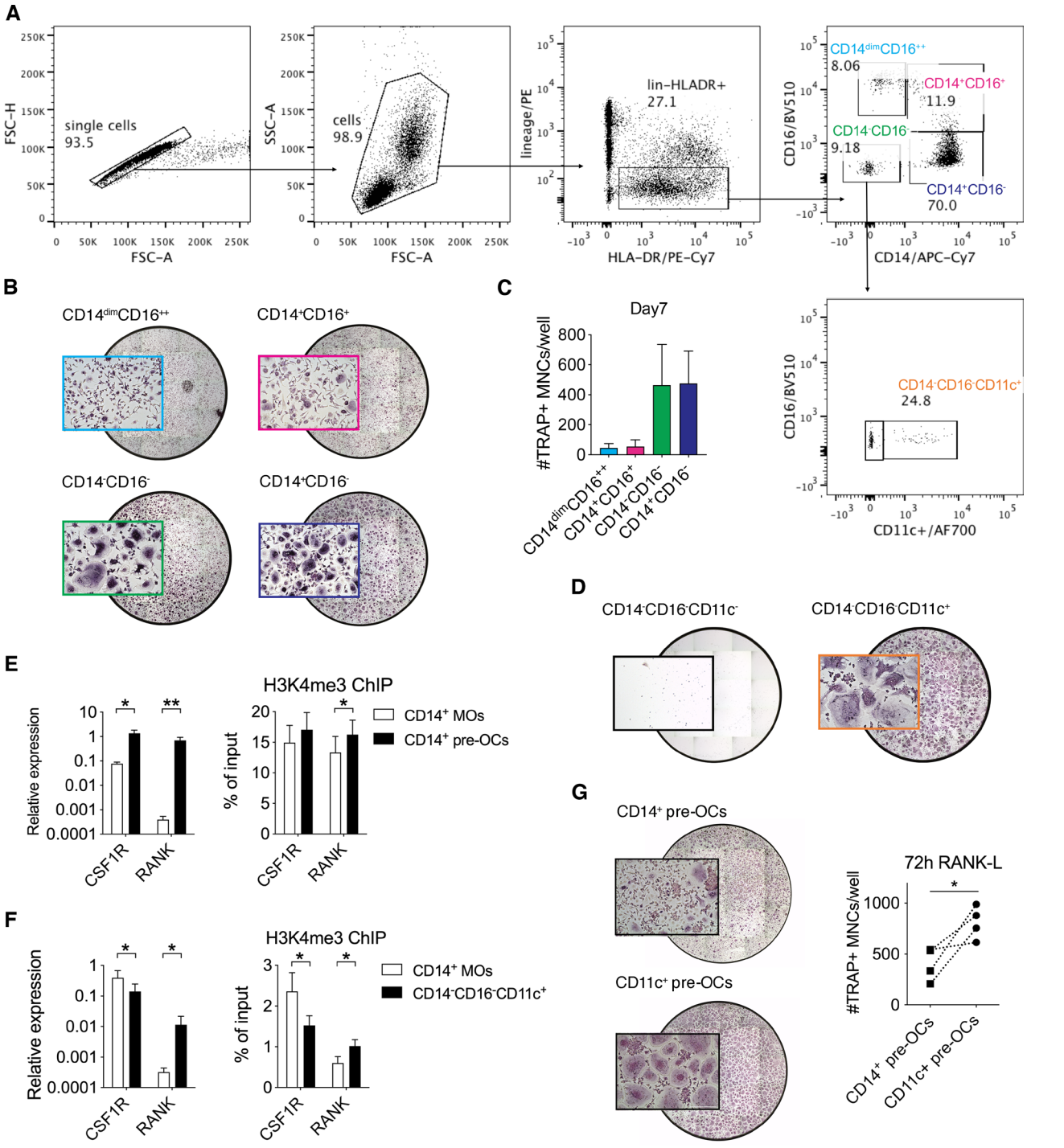


**Figure 1** Identification and epigenetic state of osteoclast (OC) precursor populations in human blood. (A–D) Sorted peripheral blood mononuclear cells (PBMCs) were plated overnight with 25 ng/mL macrophage-colony stimulating factor (M-CSF) and subsequently 25 ng/mL receptor activator of nuclear factorkappa-B ligand (RANK-L) was added to differentiate cells into OCs. At day 7 cells were fixed and stained for TRAP. (A) Representative flow cytometric plots showing the gating strategy used to sort monocyte (MO) subsets and $CD14^-CD16^-CD11c^+$ myeloid cells. Cells were pre-gated as single $Lin^-$ ($CD19^-CD3^-CD15^-CD56^-$) $HLA\text{-}DR^+$. Numbers indicate percentage of parental subset. (B) Representative digital reconstructed wells at 4× (with a boxed 10× magnification) and (C) quantification of multinucleated (nuclei ≥3) cells (MNCs) TRAP+ (purple) OC differentiated from $CD14^{dim}CD16^{++}$, $CD14^+CD16^+$, $CD14^+CD16^-$ and $CD14^-CD16^-$ subsets. (D) Representative digital images of TRAP stained wells at 4× with boxed 10× magnification images of $CD14^-CD16^-CD11c^-$ and $CD14^-CD16^-CD11c^+$ cells. (E–G) $CD14^+$ MOs and $CD14^-CD16^-CD11c^+$ precursors were magnetically enriched from PBMCs (purity ≥96%) and incubated overnight with 25 ng/mL M-CSF to generate pre-OCs. (E–F) CSF1R and RANK mRNA expression (left hand side) and ChIP assay for H3K4me3 at promoter regions (right-hand side) of CSF1R and RANK genes in either (E) $CD14^+$ MOs before and after 25 ng/mL M-CSF overnight stimulation ($CD14^+$ pre-OCs) and (F) in freshly isolated donor-matched $CD14^+$ MOS and $CD14^-CD16^-CD11c^+$ myeloid cells. Bars show mean±SD. Data were analysed with two-way analysis of variance (ANOVA) for paired data and Sidak's multiple comparisons test or paired Wilcoxon t-test (n=3–4 in E and n=6 in F). *p≤0.05; **p≤0.01. (G) Representative image of TRAP staining and quantification of TRAP+ MNCs/well of $CD14^+$ pre-OCs and $CD11c^+$ pre-OCs after 72 hours of 25 ng/mL RANK-L. Dotted lines indicate donor-matched samples. Data were analysed with Mann-Whitney test (n=4). *p≤0.05.

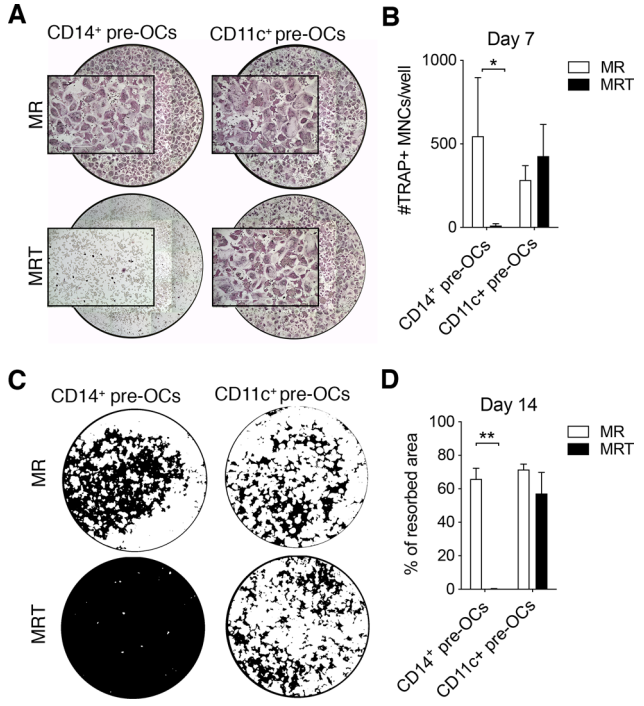


**Figure 2** Tumour necrosis factor (TNF) over-rides receptor activator of nuclear factorkappa-B ligand (RANKL)-driven osteoclastogenesis of CD14$^+$ pre-osteoclasts (OCs) but not CD11c$^+$ pre-OCs. (A–B) Freshly isolated peripheral blood mononuclear cells (PBMCs) were stained for flow cytometry and CD16$^-$CD14$^+$ monocytes (MOs) and CD14$^-$CD16$^-$CD11c$^+$ precursors were sorted, incubated overnight with 25ng/mL macrophage-colony stimulating factor to generate pre-OCs, and then differentiated into OCs for 7 days with 25 ng/mL RANK-L (MR) ±10 ng/mL TNF (MRT). (A) Representative digital reconstructed TRAP stained wells at 4× with boxed 10× magnification and (B) quantification of numbers of TRAP+ multinucleated cells (MNCs) per well. Data were analysed with two-way analysis of variance (ANOVA) and Holm-Sidak's multiple comparisons test for paired data (n=3). *p≤0.05. Error bars show mean±SD of n=3. (C–D) CD14$^+$ MOs and CD14$^-$CD16$^-$CD11c$^+$ precursors were magnetically enriched, seeded onto mineral-coated wells, and differentiated into OCs for 14 days as in (A,B). (C) Digital images of resorption pits (mineral substrate in black; resorption pits in white) and (D) % of resorption. Statistical analysis was performed using two-way ANOVA and Sidak's multiple comparisons test for paired data. Error bars=mean±SD of n=3. **p≤0.01.

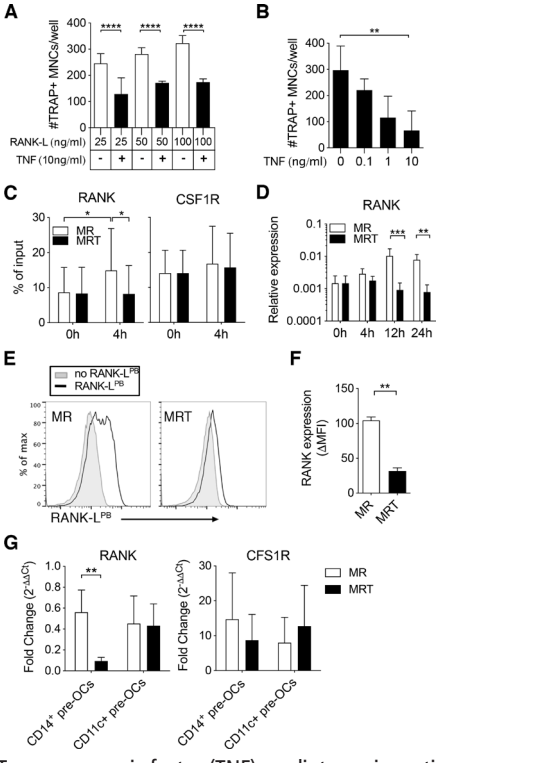


**Figure 3** Tumour necrosis factor (TNF) mediates epigenetic modification of the receptor activator of nuclear factor kappa-B (RANK) promoter and controls RANK transcription and expression in CD14$^+$ pre-osteoclasts (OCs). (A–F) Enriched CD14$^+$ monocytes (MOs) were incubated overnight with 25 ng/mL to generate CD14$^+$ pre-OCs. OCs were differentiated in the presence of RANK-ligand (RANK-L)±TNF. (A) Quantification of number of TRAP+ multinucleated cells (MNCs)/well after 6 days of culture in increasing concentrations of RANK-L (25, 50 or 100 ng/mL)±10 ng/mL TNF. Error bars show mean±SD of n=3. Data were analysed with two-way analysis of variance (ANOVA) and Tukey's multiple comparisons test. ****p≤0.0001. (B) Quantification of TRAP+ MNCs/well after 6 days of 25 ng/mL RANK-L±TNF at different concentrations (0.1, 1 or 10 ng/mL). Bars=mean±SD of n=3. Data were analysed with Friedman test with Dunn's multiple comparisons test, comparing to 0 ng/mL TNF. **p≤0.01. (C–F) CD14$^+$ pre-OCs were differentiated in the presence of 25 ng/mL macrophage-colony stimulating factor (M-CSF)+25 ng/mL RANK-L (MR) or MR +10 ng/mL TNF (MRT). (C) ChIP assay for H3K4me3 at the RANK promoter (left-hand side) and at the CSF1R promoter (right-hand side) on CD14$^+$pre-OCs (0 hour) and after 4 hours MR or MRT stimulation. Bars show mean±SD of n=4. Data were analysed with two-way ANOVA for paired data and Sidak's multiple comparisons test. *p≤0.05. (D) mRNA expression of RANK was evaluated at 0, 4, 12, and 24 hours after cytokine addition on CD14$^+$ pre-OCs. Data were analysed with two-way ANOVA and Dunnet's multiple comparisons test. **p≤0.01; ***p<0.001; n=4. (E) Representative histograms of uptake of fluorescent RANK-L (RANK-L$^{PB}$; black lines) after 72 hours of MR or MRT stimulation. Grey filled lines indicate unstained controls. (F) Graph shows quantification of RANK-L$^{PB}$ uptake; ΔMFI was calculated by subtraction of the unstained background fluorescence. Statistical significance was assessed via one-way ANOVA and Holm-Sidak's multiple comparisons test. **p≤0.01; n=3. (G) CD14$^+$ pre-OCs and CD11c$^+$ pre-OCs were stimulated with MR or MRT for 4 hours. Graphs show RANK and CSF1R mRNA fold change, calculated by normalising to values at 0 hour prior stimulation (on pre-OCs after overnight M-CSF). Statistical significance was calculated using 2-way ANOVA for paired data and Sidak's multiple comparisons test. **p≤0.01 *p≤0.05. Error bars show mean±SD of n=5.

of the TNF inhibitor etanercept[27] reversed osteoclastogenesis (online supplemental figure S3A,B).

To characterise the time-dependence of this effect of TNF, CD14$^+$ pre-OCs were stimulated with suboptimal levels of RANK-L that resulted in the appearance of mono-nucleated and bi-nucleated TRAP$^+$ cells after 72 hours stimulation. The addition of TNF at this 72 hours time-point did not inhibit osteoclastogenesis (online supplemental figure S4A,B) but rather caused an increase in OCs (online supplemental figure S4C), consistent with many previous studies.[28] Therefore, the kinetics of exposure to TNF are critical for its effect on differentiation of CD14$^+$ pre-OCs into mature OCs; with precursors initially having to commit to the OC lineage before there is a positive synergy between RANK and TNF.

To investigate the molecular mechanism responsible for early TNF exposure-mediated inhibition observed in CD14$^+$ pre-OCs, we examined the epigenetic state of the RANK promoter and the resulting transcript and protein expression. On 4 hours

stimulation with RANK-L, CD14$^+$ pre-OCs displayed enhanced H3K4me3 at the RANK promoter, with subsequent increased RANK transcript at 12 hours and 24 hours (figure 3C,D). The simultaneous addition of TNF with RANK-L suppressed this enhanced H3K4me3 and upregulation of transcript (figure 3C,D). This correlated with suppression of RANK expression at the cell surface (figure 3E,F). Notably, H3K4me3 levels at the CSF1R promoter and CSF1R transcripts were unaltered on RANK-L ±TNF stimulation (figure 3C and online supplemental figure S5). As noted before, in contrast to CD14$^+$ pre-OCs, CD11c$^+$ pre-OCs were not sensitive to the TNF inhibition (figure 2). To investigate the disconnect between the two cell types, we evaluated the transcriptional expression of RANK post-TNF treatment in donor-matched CD14$^+$ pre-OCs and CD11c$^+$ pre-OCs. Simultaneous addition of TNF with RANK-L suppressed the level of RANK in CD14$^+$ pre-OCs but not in CD11c$^+$ pre-OCs (figure 3G). Combined, these data suggest that TNF-mediated signalling in CD14$^+$-derived OC precursors, but not CD14$^-$C-D16$^-$CD11c$^+$ precursors, epigenetically modulates the RANK locus, resulting in loss of transcript and protein expression.

### TNF over-rides RANKL-driven osteoclastogenesis of CD14$^+$ circulating precursors via a TNFR1 and canonical NF-κB pathway

RANK-L and TNF belong to the same TNF superfamily; stimulation of their respective receptors results in activation of NF-κB. However, TNF stimulation of TNFR1 and TNFR2 primarily leads to activation of the canonical and non-canonical NF-κB pathways, respectively.[29 30] RANK-L stimulation of RANK predominately leads to the activation of the non-canonical NF-κB pathway.[31] TNFR1 and TNFR2 are expressed on both

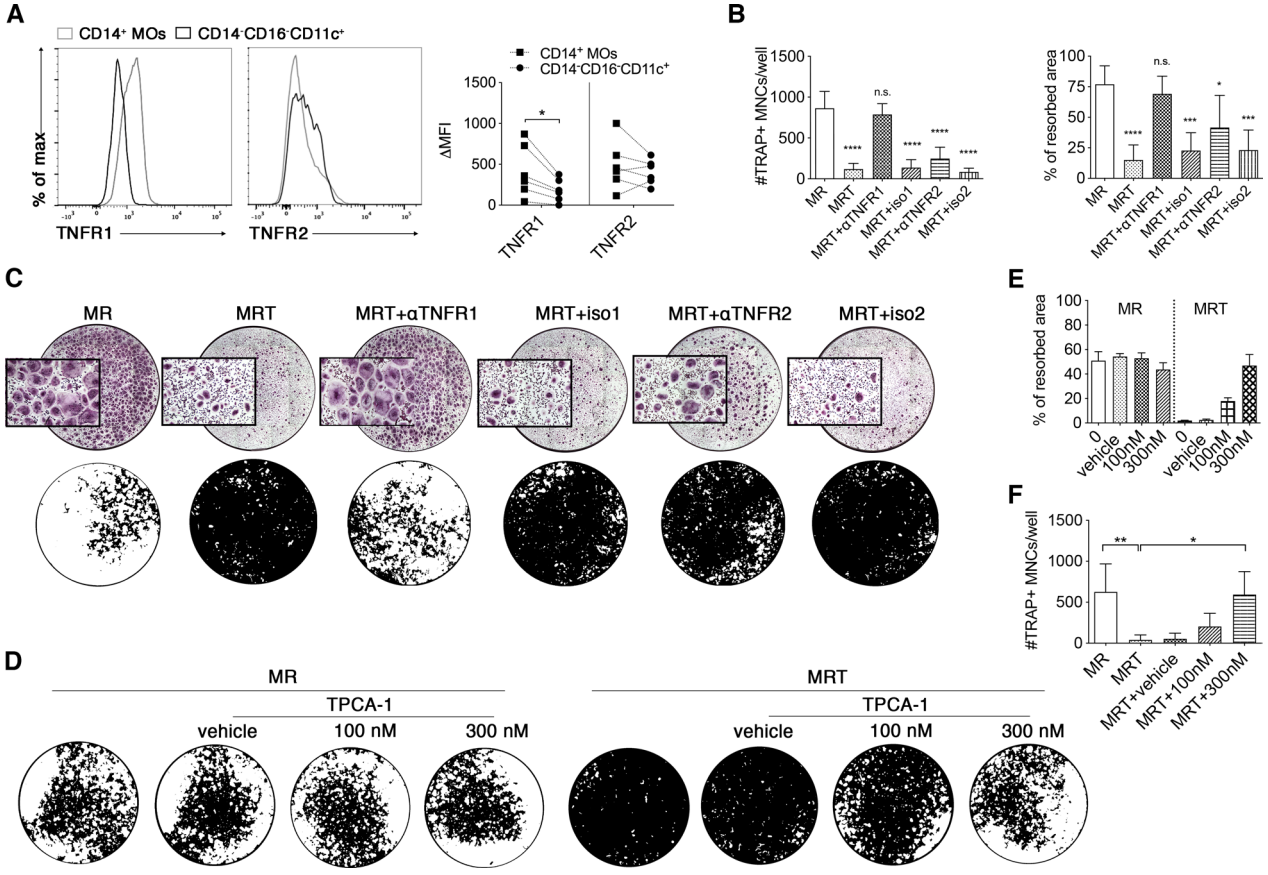


**Figure 4** Tumour necrosis factor (TNF) over-rides receptor activator of nuclear factorkappa-B ligand (RANKL)-driven osteoclastogenesis of CD14$^+$ pre-osteoclasts (OCs) via a TNFR1 and canonical NF-kB pathway. (A) Freshly isolated peripheral blood mononuclear cells (PBMCs) were stained for flow cytometry. Representative histograms showing TNFR1 and TNFR2 expression on CD14$^+$ monocytes (MOs) and CD14$^-$CD16$^-$CD11c$^+$ precursors and quantification of Δmean fluorescence intensity (MFIs) (calculated by subtracting the MFI of the TNFR to the relative MFI of the isotype control). Cells were pre-gated on single Lin$^-$(CD3$^-$CD19$^-$CD15$^-$CD56$^-$) HLA-DR$^+$. Dotted lines indicate donor-matched samples. Data were analysed with Wilcoxon matched-paired signed rank test (n=6). *p≤0.05. (B–F) CD14$^+$ pre-OCs were differentiated in the presence of 25 ng/mL macrophage-colony stimulating factor+25 ng/mL RANK-L (MR) or MR +10 ng/mL TNF (MRT). (B) Quantification of numbers of TRAP+ MNCs/well (top graph) and % of resorbed area (bottom graph) calculated, respectively at day 7 and day 10 of MR or MRT cultures±antibody blocking TNFR1 or TNFR2 (αTNFR1 and αTNFR2) or±the respective isotype controls (iso1 and iso2, respectively). Statistical significance was assessed with two-way analysis of variance (ANOVA) and Sidak's multiple comparisons test, comparing all data to MR. Error bars=mean±SD of n=3. ***p<0.001, ****p<0.0001. (C) Representative digital reconstructed wells of TRAP staining and 10× magnifications (in purple) at day 7 (top) and mineral-coated wells (mineral substrate in black; resorption pits in white) at day 10 (bottom) of CD14$^+$-derived OC culture. (D) Representative digital images of resorption assay at day 10, (E) quantification of % of resorbed area and (F) quantification of numbers of TRAP+ MNCs/well differentiated at day 7 with MR or MRT in the presence of an IKK-β inhibitor at 100 nM (MRT+100 nM) or 300 nM (MRT+300 nM) or+vehicle control (MRT+v). (E) Mean±SD of one representative experiment of n=4. Data in (F) were analysed with Friedman analysis of variance and Dunn's multiple comparisons test. *p≤0.05; **p≤0.01. Error bars indicate mean±SD of n=3.

CD14$^+$ circulating MOs and CD14$^-$CD16$^-$CD11c$^+$ myeloid cells (figure 4A).[32] However, the level of TNFR1 is significantly lower on CD14$^-$CD16$^-$CD11c$^+$ precursors (figure 4A). To assess the role of TNFR1 and TNFR2 in the TNF-mediated inhibition of OC differentiation from CD14$^+$ MOs, we utilised TNFR1-specific and TNFR2-specific blocking antibodies. Blockade of TNFR1, but not TNFR2, mitigated the inhibitory effect of TNF on OC numbers and function (figure 4B,C). Given that TNFR1-mediated signalling is through the canonical NF-κB pathway (via the IκB kinase (IKK) complex formed by IKK-α, IKK-β and NEMO),[30] we used a selective IKK-β inhibitor (TPCA-1) to specifically block this signalling cascade. Inhibition of IKK-β significantly suppressed the ability of TNF to inhibit OC differentiation and activation (figure 4D–F). Importantly, TPCA-1 did not affect RANK-L-induced osteoclastogenesis or their resorptive capacity (figure 4D,E), as this is primarily driven by non-canonical NF-κB signalling.[33–35] TNFR1-mediated signals have also been associated with initiation of caspase cascades and subsequent apoptosis. TNF stimulation of CD14$^+$ pre-OCs resulted in decreased caspase activation and no change in apoptosis levels (online supplemental figure S6). Interestingly, RANK-L-mediated differentiation of CD14$^+$ pre-OCs for 72 hours resulted in upregulation of TNFR2 (online supplemental figure S7A,B). This corresponded with TNFR2-dependent TNF-mediated enhancement of OC differentiation in these precommitted OC precursors (online supplemental figure S7C,D). Taken together, our data reveal a fundamental dual role of TNF in enhancing or blocking OC differentiation. Early exposure to concomitant RANK-L and TNF activates the canonical NF-κB pathway via TNFR1 and halts osteoclastogenesis; in contrast, later TNF addition on precommitted pre-OCs aids RANK-L and osteoclastogenesis via TNFR2 and non-canonical NF-κB signalling. This may also partly explain why circulating CD14$^-$CD16$^-$CD11c$^+$ precursors are unresponsive to TNF-mediated inhibition, given their lower levels of TNFR1 (figure 4A).

### Patients with RA have a perturbed myeloid compartment and TNF does not negatively regulate OC differentiation

Cell in the myeloid compartment and TNF play key roles in RA pathology. Analysis of circulating CD14$^+$ MOs and CD14$^-$CD16$^-$CD11c$^+$ precursors in our RA cohort showed that while the abundance of CD14$^+$ MOs was not affected in RA, CD14$^-$CD16$^-$CD11c$^+$ precursors were significantly reduced (figure 5A).

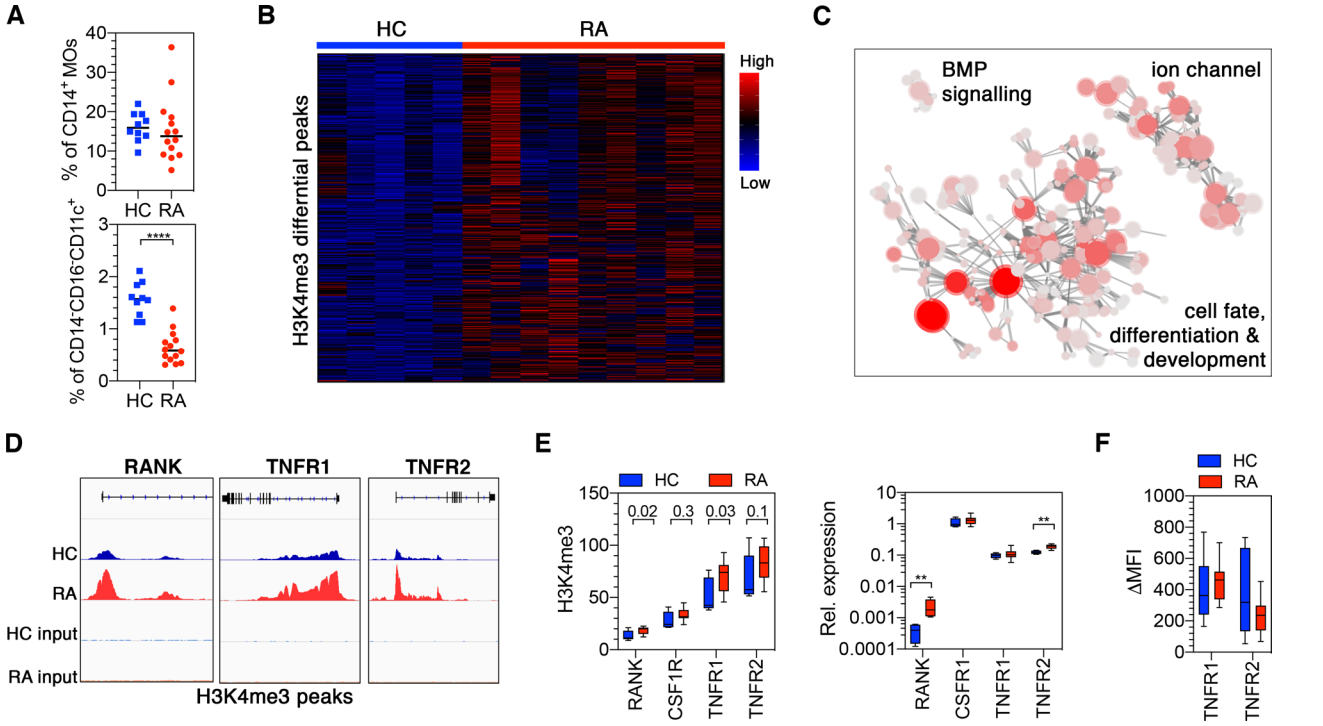


**Figure 5** Patients with rheumatoid arthritis (RA) have epigenetically perturbed CD14$^+$ monocytes with increased receptor activator of nuclear factor kappa-B (RANK) expression. (A) Freshly isolated peripheral blood mononuclear cells (PBMCs) from healthy controls (HC) and RA were stained for flow cytometry and percentages of CD14$^+$ MOs and CD14$^-$CD16$^-$CD11c$^+$ precursors in PBMCs were calculated. Statistical significance was calculated using unpaired t-test (n=10 HC and n=14 RA). ****p≤0.0001. (B) Diffbind normalised peak intensity heatmap highlighting the size and consistency of differences between HC and RA. Samples are given by column and the 6763 significantly differential peaks (<5% FDR) by row. Colour intensity indicates row scaled (z-score) peak intensity with blue as low and red as high. Rows have been hierarchically clustered using Spearman distances. (C) Network plot of the enriched (p<0.0001) Gene Ontologies for the 6763 significantly differential peaks (FDR<5%). Nodes denote Gene Ontologies and edges join nodes where >50% significant peak containing genes are shared. Node colour intensity represents enrichment (−log10p) and node size the number of significant peaks containing genes. Representative names for node clusters are given. (D) Genome Browser traces of the RANK, TNFR1 and TNFR2 H3K4me3 promoter peaks. (E) Input normalised peak intensity boxplots for the RANK, TNFR1 and TNFR2 promoter peaks (top) and relative mRNA expression measured on freshly isolated CD14$^+$ monocytes (MOs) from HC and RA (bottom). Unadjusted diffbind p values are given in the top graph. Two-way analysis of variance (ANOVA) and Sidak's multiple comparisons test was used for the analysis in the bottom graph. Graph shows box and whiskers with min to max of n=4 for HC and n=11 for RA. *p≤0.05; **p≤0.01. (F) Freshly isolated PBMCs from HC and RA were stained for flow cytometry to evaluate TNFR1 and TNFR2 expression. Box and whiskers show TNFR1 and TNFR2 expression on CD14$^+$ MOs in Δmean fluorescence intensity (MFIs) for n=13 each group. Error bars shows min to max variation.

This is consistent with previous studies showing reduced mDCs in both RA bloodstream and inflamed synovium.[36] Whether this is due to their rapid recruitment and differentiation in situ or to their minor contribution to bone erosion in RA pathology is not known. However, recent independent studies both in the blood and the synovium have interrogated the molecular signature of both $CD14^+$ MOs and CD1C pre-DC (which are the closest subset to our $CD11c^+$ myeloid precursors) in RA.[37 38] Analysis of this publicly available data revealed a high transcriptional correlation between blood and synovial CD1C cells (online supplemental figure S8A), indicating a common cell lineage origin. Notably, among the most differentially expressed gene, RANK was dramatically upregulated in the CD1C synovial counterpart, compared with circulating cells (online supplemental figure S8B). These data taken together suggest that $CD11c^+$ (or CD1C cells) are present in the inflamed synovium and have the molecular potential to differentiate into OC; although their contribution to RA bone erosion remains elusive.

In contrast, although the abundance of circulating MOs was unaffected in RA, prior studies have shown that their transcriptional profile is different from non-inflammatory controls.[39] We therefore hypothesised, having shown that the epigenetic status of $CD14^+$ MOs controls the inhibitory TNF effect, that RA blood $CD14^+$ MOs may exhibit a distinct epigenetic state. To gain further insight into this dysregulation, genome-wide H3K4me3 histone modification was investigated using ChIPseq. Comparison between patients with biological naïve RA with moderate to severe disease (DAS28=4.44±0.9) and healthy control $CD14^+$ MOs, identified 6764 significantly differential peaks (adjusted p>0.05) (figure 5B). Pathway enrichment and network analysis revealed that these differential peaks of RA MOs were primary associated with cell differentiation and development pathways (figure 5C and online supplemental dataset 1).

Based on the observed changes in RANK, CSF1R, TNFR1 and TNFR2 in healthy MOs, a focused analysis of the ChIPseq data showed that there was a significant increase of H3K4me3 in RA $CD14^+$ MOs at the RANK and TNFR1 loci but not TNFR2 and CSF1R (figure 5D,E). This corresponded with an increased level of RANK transcript but not TNFR1 (figure 5E). However, increased TNFR2 transcript was detected in RA $CD14^+$ MOs (figure 5E), although this did not correspond to a significant increase in cell surface expression (figure 5F).

Given the observed altered epigenetic landscape in RA MOs and the strong evidence that TNF drives joint destruction in RA, we hypothesised that the homoeostatic effect of TNF on circulating myeloid cells would be perturbed in RA and could thus promote OC-mediated erosive pathology. To assess the impact of this on responsiveness to TNF, $CD14^+$ pre-OCs from RA and healthy controls were differentiated in the presence of RANKL±TNF. While TNF consistently inhibited osteoclastogenesis in healthy controls, we observed a significant decrease in the capacity of TNF to inhibit osteoclastogenesis in patients with RA, with a certain degree of variance (figure 6A). In particular, 44% manifest TNF-mediated inhibition (responders), whereas in 56% of patients TNF was unable to inhibit osteoclastogenesis (non-responders; figure 6A,B). Remarkably, TNF had an enhancing pro-osteoclastogenic effect in 45% of the non-responder group. To further investigate the heterogeneity in the patients with RA, ChIPseq data of those patients that showed TNF-mediated inhibition (responders) and those that did not (non-responders) were compared. This analysis revealed that there were 4172 significantly differential peaks (figure 6C). Pathway enrichment showed that abundant peaks in RA MOs of the non-responder group were associated with transmembrane receptor protein kinase pathways and DNA-binding transcription repressor activity pathways (figure 6D and online supplemental dataset 2). Among the transmembrane receptor protein kinase pathways, CSF1R was found to be lower in the non-responders compared with the responders. STRING analysis of the identified transmembrane receptor protein kinase pathway associated genes also provided a link between CSF1R and NRP1 (figure 6E). Interestingly, NRP1 is known to act as a coreceptor for vascular endothelial growth factor (VEGF)-R[40] in MOs/macrophage, and VEGFR expression and VEGF-mediated signalling has been associated with MO differentiation into OCs.[41 42] Evaluation of RA patient serum revealed that high levels of VEGF correlate with response to TNF (figure 6F). Combined, these data suggest that in a proportion of patients with RA the high levels of VEGF correlate with a perturbation in the myeloid compartment, such that TNF homoeostatic control is diminished, thereby enhancing the potential for maturation of OCs derived from the circulating MO pool when they enter the joint.

## DISCUSSION

Our data reveal an unexpected role for TNF in the control of cell fate decisions in the myeloid compartment that regulates OC development and subsequent activation. In homoeostatic conditions, TNF can directly over-ride OC differentiation signals to which circulating myeloid precursors would otherwise respond. Furthermore, we have identified a specific human $Lin^-HLA^-DR^+CD14^-CD16^-CD11c^+$ precursor population that preferentially differentiates down the OC lineage, and that, based on its epigenetic state, is unresponsive to homoeostatic regulation imparted by TNF. In RA, a proportion of patients with moderate/severe disease activity exhibit failure of this regulatory role of TNF with some patients even exhibiting accelerated osteoclastogenesis on TNF exposure at this very early time point in the precursor differentiation pathway. This perturbed response is due to an altered MO epigenetic landscape. Taken together, our findings provide a novel, previously unrecognised hierarchy between TNF cytokine family members regulating cell fate decisions in both health and disease, which is mediated via the epigenetic set-point of circulating precursors defining their capacity to respond to cytokine combinations in the local milieu.

Our finding that homoeostatic TNF can control MO, but not other myeloid precursor differentiation in osteoclastogenic rich environments defines a paradigm in which priming of cells within the circulating myeloid compartment creates either a permissive or non-permissive epigenetic state that allows cells to differentiate down the most appropriate lineage. It is however, currently unclear how this epigenetic state is achieved in circulating MOs or how TNF drives additional changes, and thus the role of specific histone methyltransferase and/or demethylases should be evaluated in future studies.[43] Previous studies have demonstrated that $CD14^+$ MO-derived immature DC-like cells have the ability to transdifferentiate into OCs more efficiently than $CD14^+$ MO progenitors.[19 44] Note however, that circulating pre-DCs are the only cell subset capable of generating classical DCs while $CD14^+$ MO can only generate DC-like cells.[7] Our findings provide the first evidence that circulating human $Lin^-HLA^-DR^+CD14^-CD16^-CD11c^+$, which can also phenotypically be associated with the pre-DC population, can differentiate down the OC lineage. Whether $Lin^-HLA^-DR^+CD14^-CD16^-CD11c^+$/pre-DCs are the missing OC precursor in humans remains to be conclusively determined.

Based on this work, we suggest that in a normal self-resolving inflammatory event (which can include sterile/acute

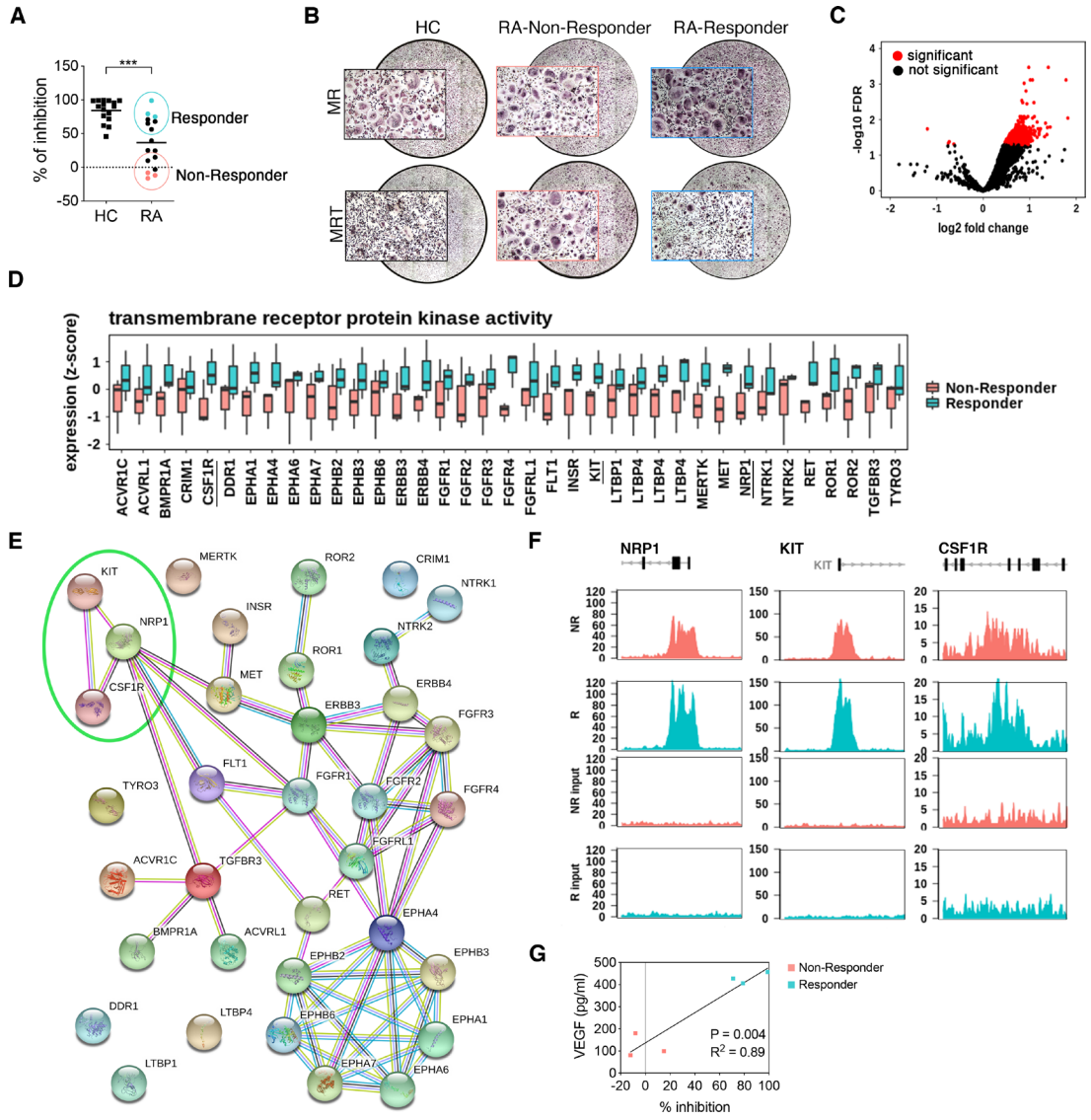


**Figure 6** Tumour necrosis factor (TNF) does not inhibit CD14$^+$-derived osteoclast (OC) differentiation in a portion of patients with rheumatoid arthritis (RA). (A–B) CD14$^+$ pre-OCs were differentiated for 7 days into OCs in the presence of 25 ng/mL macrophage-colony stimulating factor (M-CSF) and receptor activator of nuclear factorkappa-B ligand (RANK-L) (MR) ±10 ng/mL TNF (MRT). (A) Percentage of inhibition of OC differentiation was calculated as 100–[(100×#OCs$_{(MRT)}$)/#OCs$_{(MR)}$] in patients with healthy controls (HC) and RA. Light red dots indicate non-responder group and light blue dots the responder using in subsequent ChIP analysis. Data were analysed with Mann Whitney test (n=16). **p≤0.01. (B) Representative reconstructed wells and 10× magnifications of TRAP staining of one representative HC, one RA non-responder and one RA responder, in MR and MRT conditions. OCs=TRAP+ multinucleated cells, MR=M-CSF+RANK L, MRT=M-CSF+RANK-L+TNF. (C) Volcano plot for RA responders versus non-responders across the 65 717 consensus peaks. Significantly differential peaks (<5% FDR) are highlighted in red. Positive fold changes denote greater peak intensity in RA responders. (D) Boxplot of the 35 significantly differential peaks (<5% FDR) between RA non-responders and RA responders that are associated with the top enriched (p<0.0001) gene ontology transmembrane receptor protein kinase activity. Individual peaks (and the gene they are associated with) are given on the x-axis and the Diffbind normalised peak intensity (per peak z-score) is given on the y-axis. Separate boxes are provided for non-responder samples (n=3) and responder samples (n=3). (E) STRING network plot of the genes in the transmembrane receptor protein kinase activity gene ontology. Nodes represent proteins and edges joining nodes represent protein–protein associations (known interactions; blue—curated data, pink—experimentally determined. Predicted interactions; green—gene neighbours. Other interaction; black—coexpression). Genes of interest are circled in green. (F) Correlation analysis between % of inhibition of OC differentiation and serum vascular endothelial growth factor (VEGF) concentration.

inflammation), Lin$^-$HLA$^-$DR$^+$CD14$^-$CD16$^-$CD11c$^+$ cells recruited to bone will still respond to the cytokine rich local environment by differentiating down the OC lineage and thus help maintain skeletal health. In contrast, circulating CD14$^+$ MOs are in a non-permissive state and are inhibited from contributing to the OC pool. We recognise the limitations of our study; in that we have used in vitro methods to evaluate cell fate decisions within the myeloid compartment. Evidence to further support this theory would require human in vivo/ex vivo cell fate mapping studies to determine which precursors (Lin$^-$HLA$^-$DR$^+$CD14$^-$CD16$^-$CD11c$^+$ or CD14$^+$ MOs) contribute to the bone-associated OC pool. Unfortunately, these assays are not currently possible. Further studies will need to define a way of identifying Lin$^-$HLA$^-$DR$^+$CD14$^-$CD16$^-$CD11c$^+$—versus MO-derived OCs in situ to better understand this alternative route to mature OCs. Moreover, they

should also investigate the global molecular and epigenetic signature of $Lin^{-}HLA^{-}DR^{+}CD14^{-}CD16^{-}CD11c^{+}$ and $CD14^{+}$ precursors cells, and their respective mature OCs, to ultimately identify the specific precursor cells and molecular mechanisms involved in inflammatory joint destruction.

Anti-TNF therapy is one of the gold standard treatments for multiple inflammatory-mediated diseases including RA. It is paradoxical however, given that TNF inhibitors are known to be antierosive,[45] that we show an antierosive effect for TNF itself via a homoeostatic pathway in health. Crucially, we do show that in a proportion of patients with RA with have higher levels of VEGF, there is a failure in this homoeostatic pathway. Leading us to hypothesise that such failure may represent a route MO preconditioning and subsequent accelerated erosion in a subset of patients. Characterising the nature of such a failure may offer future therapeutic opportunities. For instance, determining how to re-engage this regulatory pathway may lead to new antierosive therapeutics that have the ability to re-sensitise some patients with RA to the regulatory element of TNF biology. This could also have the added value of reducing the capacity of TNF, produced for example during RA synovitis, to sensitise early precursors down the OC pathway. Finally, the newly identified $Lin^{-}HLA^{-}DR^{+}CD14^{-}CD16^{-}CD11c^{+}$ precursor route to mature OCs represents an unexplored independent mechanism to mature OCs and potentially erosive progression in RA. A detailed understanding of this new pathway could reveal an as yet untargeted pathway in the disease context. In summary, these data support further evaluation of these pathways in RA and other diseases associated with bone pathology to discover their utility as alternative therapeutic strategies to abrogate erosive progression.

**Twitter** Stefan Siebert @StefanSiebert1 and Carl S Goodyear @carl_goodyear

**Acknowledgements** We thank the patients with RA and healthy donors who participated in this study.

**Contributors** CA, IM and CSG conceived and designed the concepts, experiments, data analysis and overall research. IM and CSG directed the research. CA, FS, SC, performed experiments and data analysis. JC performed the bioinformatic analyses. SSood helped with sample processing and technical troubleshooting. JR and SSiebert collected clinical samples and provided assistance in clinical interpretation. CA, IM and CSG wrote the manuscript with the input of the other authors.

**Funding** The work was supported by European Commission Seventh Framework Programme and Marie Curie Actions (project Osteoimmune; FP7-PEO- PLE-2011-ITN-289150) with additional support by ARUK Centre of Excellence for the Pathogenesis of Rheumatoid Arthritis (RACE/#20298). FS was supported by an ARTICULUM Fellowship.

**Competing interests** None declared.

**Patient consent for publication** Not required.

**Provenance and peer review** Not commissioned; externally peer reviewed.

**Data availability statement** Data are available in a public, open access repository. Data and materials availability: ChIP-seq datasets were deposited in Gene Expression Omnibus (GEO) with the accession number ID GSE15291 and token irctaigmjlmxtkj (https://www.ncbi.nlm.nih.gov/geo/query/acc.cgi?acc=GSE152912)



**ORCID iDs**
Cecilia Ansalone http://orcid.org/0000-0001-8683-1718
Jamie Robertson http://orcid.org/0000-0003-2575-9331
Carl S Goodyear http://orcid.org/0000-0001-5926-5941

## REFERENCES

1 Jacome-Galarza CE, Percin GI, Muller JT, *et al*. Developmental origin, functional maintenance and genetic rescue of osteoclasts. *Nature* 2019;568:541–5.
2 Boyle WJ, Simonet WS, Lacey DL. Osteoclast differentiation and activation. *Nature* 2003;423:337–42.
3 Li J, Sarosi I, Yan XQ, *et al*. Rank is the intrinsic hematopoietic cell surface receptor that controls osteoclastogenesis and regulation of bone mass and calcium metabolism. *Proc Natl Acad Sci U S A* 2000;97:1566–71.
4 Jacome-Galarza CE, Lee S-K, Lorenzo JA, *et al*. Identification, characterization, and isolation of a common progenitor for osteoclasts, macrophages, and dendritic cells from murine bone marrow and periphery. *J Bone Miner Res* 2013;28:1203–13.
5 Rivollier A, Mazzorana M, Tebib J, *et al*. Immature dendritic cell transdifferentiation into osteoclasts: a novel pathway sustained by the rheumatoid arthritis microenvironment. *Blood* 2004;104:4029–37.
6 Guilliams M, Ginhoux F, Jakubzick C, *et al*. Dendritic cells, monocytes and macrophages: a unified nomenclature based on ontogeny. *Nat Rev Immunol* 2014;14:571–8.
7 Villani A-C, Satija R, Reynolds G, *et al*. Single-cell RNA-seq reveals new types of human blood dendritic cells, monocytes, and progenitors. *Science* 2017;356. doi:10.1126/science.aah4573. [Epub ahead of print: 21 Apr 2017].
8 Charles JF, Hsu L-Y, Niemi EC, *et al*. Inflammatory arthritis increases mouse osteoclast precursors with myeloid suppressor function. *J Clin Invest* 2012;122:4592–605.
9 Komine M, Kukita A, Kukita T, *et al*. Tumor necrosis factor-alpha cooperates with receptor activator of nuclear factor kappaB ligand in generation of osteoclasts in stromal cell-depleted rat bone marrow cell culture. *Bone* 2001;28:474–83.
10 Lam J, Takeshita S, Barker JE, *et al*. TNF-α induces osteoclastogenesis by direct stimulation of macrophages exposed to permissive levels of RANK ligand. *J Clin Invest* 2000;106:1481–8.
11 Zhang YH, Heulsmann A, Tondravi MM, *et al*. Tumor necrosis factor-alpha (TNF) stimulates RANKL-induced osteoclastogenesis via coupling of TNF type 1 receptor and RANK signaling pathways. *J Biol Chem* 2001;276:563–8.
12 Kalliolias GD, Ivashkiv LB. TNF biology, pathogenic mechanisms and emerging therapeutic strategies. *Nat Rev Rheumatol* 2016;12:49–62.
13 Keffer J, Probert L, Cazlaris H, *et al*. Transgenic mice expressing human tumour necrosis factor: a predictive genetic model of arthritis. *Embo J* 1991;10:4025–31.
14 Manara M, Sinigaglia L. Bone and TNF in rheumatoid arthritis: clinical implications. *RMD Open* 2015;1:e000065.
15 Shi C, Pamer EG. Monocyte recruitment during infection and inflammation. *Nat Rev Immunol* 2011;11:762–74.
16 Massey HM, Flanagan AM. Human osteoclasts derive from CD14-positive monocytes. *Br J Haematol* 1999;106:167–70.
17 Komano Y, Nanki T, Hayashida K, *et al*. Identification of a human peripheral blood monocyte subset that differentiates into osteoclasts. *Arthritis Res Ther* 2006;8:R152.
18 Tinkler SM, Linder JE, Williams DM, *et al*. Formation of osteoclasts from blood monocytes during 1 alpha-OH Vit D-stimulated bone resorption in mice. *J Anat* 1981;133:389–96.
19 Gallois A, Lachuer J, Yvert G, *et al*. Genome-wide expression analyses establish dendritic cells as a new osteoclast precursor able to generate bone-resorbing cells more efficiently than monocytes. *J Bone Miner Res* 2010;25:661–72.
20 MacLellan LM, Montgomery J, Sugiyama F, *et al*. Co-opting endogenous immunoglobulin for the regulation of inflammation and osteoclastogenesis in humans and mice. *Arthritis Rheum* 2011;63:3897–907.
21 Arai F, Miyamoto T, Ohneda O, *et al*. Commitment and differentiation of osteoclast precursor cells by the sequential expression of c-fms and receptor activator of nuclear factor kappaB (RANK) receptors. *J Exp Med* 1999;190:1741–54.
22 Dong X, Weng Z. The correlation between histone modifications and gene expression. *Epigenomics* 2013;5:113–6.
23 Ichikawa K, Liu W, Fleck M, *et al*. TRAIL-R2 (DR5) mediates apoptosis of synovial fibroblasts in rheumatoid arthritis. *J Immunol* 2003;171:1061–9.
24 Redlich K, Hayer S, Maier A, *et al*. Tumor necrosis factor alpha-mediated joint destruction is inhibited by targeting osteoclasts with osteoprotegerin. *Arthritis Rheum* 2002;46:785–92.
25 Redlich K, Hayer S, Ricci R, *et al*. Osteoclasts are essential for TNF-alpha-mediated joint destruction. *J Clin Invest* 2002;110:1419–27.
26 Li P, Schwarz EM. The TNF-alpha transgenic mouse model of inflammatory arthritis. *Immunopathol* 2003;25:19–33.
27 Moreland LW, Baumgartner SW, Schiff MH, *et al*. Treatment of rheumatoid arthritis with a recombinant human tumor necrosis factor receptor (p75)-Fc fusion protein. *N Engl J Med* 1997;337:141–7.

28 Lee SE, Chung WJ, Kwak HB, *et al*. Tumor necrosis factor-alpha supports the survival of osteoclasts through the activation of Akt and ERK. *J Biol Chem* 2001;276:49343–9.
29 Oeckinghaus A, Hayden MS, Ghosh S. Crosstalk in NF-κB signaling pathways. *Nat Immunol* 2011;12:695–708.
30 Sun S-C. The non-canonical NF-κB pathway in immunity and inflammation. *Nat Rev Immunol* 2017;17:545–58.
31 Boyce BF, Xiu Y, Li J, *et al*. NF-κB-Mediated Regulation of Osteoclastogenesis. *Endocrinol Metab* 2015;30:35–44.
32 Hijdra D, Vorselaars AD, Grutters JC, *et al*. Differential expression of TNFR1 (CD120a) and TNFR2 (CD120b) on subpopulations of human monocytes. *J Inflamm* 2012;9:38.
33 Novack DV, Yin L, Hagen-Stapleton A, *et al*. The IκB function of NF-κB2 p100 controls stimulated osteoclastogenesis. *J Exp Med* 2003;198:771–81.
34 Vaira S, Johnson T, Hirbe AC, *et al*. Relb is the NF-kappaB subunit downstream of NIK responsible for osteoclast differentiation. *Proc Natl Acad Sci U S A* 2008;105:3897–902.
35 Zhao Z, Hou X, Yin X, *et al*. Tnf induction of NF-κB RelB enhances RANKL-induced osteoclastogenesis by promoting inflammatory macrophage differentiation but also limits it through suppression of NFATc1 expression. *PLoS One* 2015;10:e0135728.
36 Jongbloed SL, Lebre MC, Fraser AR, *et al*. Enumeration and phenotypical analysis of distinct dendritic cell subsets in psoriatic arthritis and rheumatoid arthritis. *Arthritis Res Ther* 2006;8:R15.
37 Canavan M, Marzaioli V, McGarry T, *et al*. Rheumatoid arthritis synovial microenvironment induces metabolic and functional adaptations in dendritic cells. *Clin Exp Immunol* 2020;202:226–38.
38 Zhang F, Wei K, Slowikowski K, *et al*. Defining inflammatory cell states in rheumatoid arthritis joint synovial tissues by integrating single-cell transcriptomics and mass cytometry. *Nat Immunol* 2019;20:928–42.
39 Smiljanovic B, Radzikowska A, Kuca-Warnawin E, *et al*. Monocyte alterations in rheumatoid arthritis are dominated by preterm release from bone marrow and prominent triggering in the joint. *Ann Rheum Dis* 2018;77:300–8.
40 Casazza A, Laoui D, Wenes M, *et al*. Impeding macrophage entry into hypoxic tumor areas by Sema3A/Nrp1 signaling blockade inhibits angiogenesis and restores antitumor immunity. *Cancer Cell* 2013;24:695–709.
41 Niida S, Kaku M, Amano H, *et al*. Vascular endothelial growth factor can substitute for macrophage colony-stimulating factor in the support of osteoclastic bone resorption. *J Exp Med* 1999;190:293–8.
42 Sawano A, Iwai S, Sakurai Y, *et al*. Flt-1, vascular endothelial growth factor receptor 1, is a novel cell surface marker for the lineage of monocyte-macrophages in humans. *Blood* 2001;97:785–91.
43 Hyun K, Jeon J, Park K, *et al*. Writing, erasing and reading histone lysine methylations. *Exp Mol Med* 2017;49:e324.
44 Alnaeeli M, Park J, Mahamed D, *et al*. Dendritic cells at the osteo-immune interface: implications for inflammation-induced bone loss. *J Bone Miner Res* 2007;22:775–80.
45 Combe B, Lula S, Boone C, *et al*. Effects of biologic disease-modifying anti-rheumatic drugs on the radiographic progression of rheumatoid arthritis: a systematic literature review. *Clin Exp Rheumatol* 2018;36:658–67.

**Online Supplementary Materials**

# TNF is a homeostatic regulator of distinct epigenetically primed human osteoclast precursors

**Authors:** Cecilia Ansalone, John Cole, Sabarinadh Chilaka, Flavia Sunzini, Shatakshi Sood, Jamie Robertson, Stefan Siebert, Iain B. McInnes, and Carl S. Goodyear.

## Contents





Ansalone C, *et al. Ann Rheum Dis* 2021;0:1–10. doi: 10.1136/annrheumdis-2020-219262

- Pg 23: Table S1. RA patient's characteristics. Table S2. Primer sequences used for quantitative RT-PCR. Table S3. Primer sequences used for ChIP-PCR of promoter regions of selected genes. References.



Ansalone C, *et al. Ann Rheum Dis* 2021;0:1–10. doi: 10.1136/annrheumdis-2020-219262

**Supplementary materials and methods**

*Blood collection and cell isolation*

Blood from healthy individuals and RA patients was collected in lithium heparin vacuum blood tubes (BD Vacutainer LH, 170 IU). For certain RA patients, blood for serum separation was also collected (BD Vacutainer SST II Advance). Blood samples from patients diagnosed with RA (with a diagnosis meeting the 2010 ACR/EULAR RA criteria) were collected at Rheumatology clinics (Glasgow, UK); all patients were naïve to TNF-biologics and had moderate to severe disease based on their Disease Activity Score (DAS28). Table S1 summarizes the characteristics of our study population. The study protocol was approved by the West of Scotland Research Ethical Committee (11/S0704/7). All the donors provided signed informed consent. Alternatively, buffy coat was obtained from the Scottish National Blood Transfusion Service (approved by Glasgow NHS Trust-East Ethics Committee). Peripheral blood mononuclear cells (PBMCs) were extracted by density gradient separation using Ficoll-paque PLUS (GE Healthcare Life Science). $CD14^+$ monocytes and $CD11c^+$ precursors were magnetically enriched from PBMCs using EasySep™ Human CD14 Positive Selection Kit and EasySep™ Human Myeloid DC Enrichment Kit (STEMCELL Technologies) respectively. Purity was assessed via flow cytometry staining and showed purity≥96%.

*Cell cultures and osteoclast differentiation and analysis*

Freshly isolated PBMCs, magnetically enriched $CD14^+$ monocytes and $CD11c^+$ precursors (purity≥96%), as well as fluorescently sorted populations (purity≥99%), were re-suspended at $1x10^6$/ ml in complete α-MEM medium (supplemented with 10% of heat inactivated foetal bovine serum (FBS), 0.02 mML-glutamine, 10 units/ml penicillin, 0.1

mg/ml streptomycin) (Invitrogen, Thermo Fisher Scientific), plated at density of $1x10^5$/well in 96-well plates either on plastic or on mineral-coated plates (Corning osteo-assay surface microplate) and stimulated with 25 ng/ml macrophage–colony-stimulating factor (M-CSF; Peprotech). After overnight incubation cells were defined as $CD14^+$ pre-osteoclasts (pre-OCs) and $CD11c^+$ pre-OCs (approximately 18h) and used for down-stream applications. Osteoclasts were differentiated by stimulating pre-OCs with 25ng/ml (unless where otherwise stated) receptor activator of nuclear factor kappa-B ligand (RANK-L), alongside 25ng/ml M-CSF. Tumor necrosis factor alpha (TNF) was used at 0.1, 1, and 10 ng/ml and added at different time points during osteoclastogenesis, as specified in figure legends. Medium was refreshed every 3-4 days. For cultures on plastic, osteoclast differentiation was assessed by fixation of cells and staining with tartrate-resistant acid phosphatase (TRAP) kit (Sigma-Aldrich), in accordance with the manufacturer's instructions. For the resorption assay, cells were removed from mineral-coated plates using a 10-15% sodium hypochlorite solution (Sigma-Aldrich) and the mineral substrate left to air dry. Reconstructed digital images of the entire well were acquired using an EVOS FL Auto Cell Imaging System (Life Technologies). Osteoclasts were identified as $TRAP^+$ multinucleated (nuclei≥3) cells (MNCs) and counted using Fiji software (ImageJ). Resorption was calculated using Fiji software (ImageJ) by converting the images into 8-bit and setting the threshold at 223 to 254; resorption areas were calculated as % of the total area of the well.

*Signalling inhibition and TNF receptor blockade during osteoclastogenesis*

TNF receptor fusion protein etanercept (Enbrel, Amgen) was added to osteoclast cultures at 1, 10, or 50 μg/ml alongside with TNF. Additionally, purified antibody specifically recognizing TNF receptor 1 (mouse anti-human CD120a; αTNFR1; eBioscience) and TNF receptor 2 (rat anti- human CD120b; αTNFR2; BioLegend) were added to

osteoclast cultures in the presence of RANK-L ± TNF. Appropriate isotype antibody controls were purchased from BioLegend and used as negative controls. All antibodies and isotypes were used at 10 μg/ml. In some experiments, TPCA-1 ([5-(p-Fluorophenyl)-2-ureido]thiophene-3-carboxamide; Sigma-Aldrich) was used to specifically inhibit IκB kinase-2 (IKK-2; IC50 = 17.9 nM). TPCA-1 was added at 100 and 300nM at the beginning of the osteoclast culture alongside 25 ng/ml RANK-L ± 10 ng/ml TNF. After 24h the inhibitor was washed off and medium replaced with 25 ng/ml RANK-L ± 10 ng/ml TNF. 0.06% Dimethyl sulfoxide (DMSO) was used as vehicle control.

*Cell preparation for flow cytometry applications*

Freshly isolated PBMCs were suspended in DPBS supplemented with 1% FBS, 0.1% $NaN_3$ and 5mM EDTA and stained for flow cytometry. Alternatively, freshly enriched $CD14^+$ monocytes were incubated overnight with 25ng/ml M-CSF to generate $CD14^+$ pre-OCs (0h) and then stimulated with 25 ng/ml RANK-L ± 10 ng/ml TNF for 72h. Control wells received M-CSF alone. Cell were taken at 0 and 72h and stained for flow cytometry. To sort specific populations, PBMCs were stained with flow cytometry antibodies in sterile DPBS supplemented with 1% FBS and 2mM EDTA and sorted using an BD FACSAria III cell sorter with an 85μm nozzle (BD Bioscience). Cells were sorted into tubes containing complete α-MEM, re-suspended at $1x10^6$ cells/ml and incubated overnight with 25ng/ml M-CSF for downstream osteoclast cultures. Post-sorting check assessed purity≥99%. Antibody staining was performed in the dark for 15 minutes at 4˚C. Additional incubation for 20 minutes at 4˚C with PerCP/Cy5.5 Streptavidin (BioLegend) was performed where required. Washed cells were acquired with an LSR II cytometer (BD Bioscience) and data analysed with a Flowjo 10.0.5 software (Tree Star).

*Antibodies used for flow cytometry*

Anti-human antibodies used for flow cytometry applications are listed below: APC-Cy7 CD14 (M5E2; BioLegend), PE-CF594 mouse anti-human CD14 (MφP9; BD Bioscience), V500 CD16 (3G8; BD Biosciences), PE-Cy7 HLA-DR (G46-6; BD Biosciences); Alexa Fluor-700 CD11c (B-ly6; BD Bioscience), Brilliant Violet-605 CD123 (6H6; BioLegend), biotin TNFR1/CD120a (MABTNFR1-B1; BD Bioscience), Alexa Fluor-647 TNFR2/CD120b (hTNFR-M1; BD Bioscience), PE CD3 (UCHT1; BD Bioscience), PE CD19 (J3-119; Beckman Coulter), PE CD56 (MY31; BD Biosciences); PE CD15 (VIMC6; Miltenyi Biotec); APC CD80 (2D10; BioLegend); FITC CD64 (10.1; BioLegend); Brilliant Violet 421 CD206 (15-2; BioLegend). Mouse IgG2a (G155-178; BD Bioscience) and rat IgG2a (A95-18; BD Biosciences) were used as isotype controls for TNFR1 and TNFR2 respectively.

*Labelling of RANK-L and fluorescent protein up-take*

Recombinant human soluble RANK-L (Peprotech) was re-suspended at 1 mg/ml in $dH_2O$ and labelled with Pacific Blue™ protein labelling kit, following the manufacturer's instructions (Thermo Fisher Scientific). Concentration of the labelled cytokine ($RANK\text{-}L^{PB}$) was assessed by Nanodrop and adjusted to 100μg/ml in 0.1% bovine serum albumin (BSA) in Dulbecco's phosphate-buffered saline (DPBS; Life Technologies, Thermo Fisher Scientific).

$CD14^+$ monocytes were differentiated into OCs for 72h in the presence of 25 ng/ml RANK-L ± 10 ng/ml TNF and then incubated at 37˚C for 1 hour with 100ng/$1x10^6$ cells $RANK\text{-}L^{PB}$ in complete α-MEM medium (no FBS). Medium alone was used as negative control. After the incubation, cells were washed and re-suspended in DPBS supplemented

with 1% FBS, 0.1% $NaN_3$ and 5mM Ethylene-di-amine-tetra-acetic acid (EDTA) for flow cytometry analysis.

*Cytokine production analysis*

$CD14^+$ monocytes, after overnight incubation, were stimulated with different combinations of 25ng/ml M-CSF, 25ng/ml RANKL, and 10ng/ml TNF. Granulocyte macrophage colony-stimulating factor (GM-CSF; Peprotech) was used at 100 ng/ml. After 6 days medium was removed and replaced with media containing vehicle control or 100ng/ml lipopolysaccharide (LPS from Salmonella Minnesota R595; InvivoGen). After 18h supernatants were stored, and cytokine production was assessed. Alternatively, $CD14^+$ monocytes and $CD11c^+$ precursors were magnetically enriched, incubated overnight with 25ng/ml M-CSF to generate pre-OCs and then stimulated for 72h with 25ng/ml RANKL ± 10ng/ml TNF. Supernatants were collected and cytokine concentration assessed using the Meso Scale Discovery technology (Meso Scale Diagnostics). Specifically, a V-PLEX Pro-inflammatory Panel 1 Human Kit (Meso Scale Diagnostics) was used to determine concentrations of IL-10, IL-12p70, IL-1β, IL-6, and IFNγ in cell supernatants, following manufacturer's instructions. Analysis was performed using the MSD Discovery Workbench analysis software (Meso Scale Diagnostics).

*RNA isolation and quantitative RT-PCR*

Cells were lysed in RLT buffer (Qiagen) containing 1% beta-mercaptoethanol. mRNA was extracted according to the manufacturer's instructions using the RNeasy Micro Kit (Qiagen) and eluted in 15 µl RNAse-free $H_2O$. cDNA was synthesized using High capacity cDNA reverse transcription kit (Applied Biosystems, Thermo Fisher Scientific). A

quantity of 1 ng cDNA was taken for RT-qPCR analysis using Power SYBR Green PCR Master Mix (Applied Biosystems, Thermo Fisher Scientific), and a QuantStudio 6 machine (Thermo Fisher Scientific). A quantity of 1 ng cDNA was taken for RT-qPCR analysis using Power SYBR Green PCR Master Mix (Applied Biosystems, Thermo Fisher Scientific), and a QuantStudio 6 machine (Thermo Fisher Scientific). Relative gene expression and fold change was calculated using the comparative $C_T$ method[1]. $\Delta C_T$ values were calculated as $C_{T\ \text{gene of interest}} - C_{T\ \text{housekeeping gene}}$ for each sample. The $\Delta C_T$ is then converted to linear relative gene expression using the following formula $2^{-\Delta CT}$. Fold change was measured as $2^{-\Delta\Delta CT}$, where $\Delta\Delta C_T$ corresponded to $\Delta C_{T\ \text{control sample}} - \Delta C_{T\ \text{treated sample}}$. Oligonucleotides were designed in house and listed in Table S2. Primers for RANK and GAPDH were designed on exon span junctions. In order to avoid genomic contamination, endogenous DNA was digested using RNase-Free DNase set during mRNA extraction, as described in the manufacturer's instructions (Qiagen).

*Chromatin Immunoprecipitation (ChIP)*

Cells were fixed in 1% formaldehyde for 10 minutes at room temperature, followed by quenching with 125mM Glycine for 5 minutes. Cells were scraped and collected by centrifugation at 4˚C. Pelleted cells were washed twice with cold DPBS (GIBCO, Thermo Fisher Scientific) and lysed in lysis buffer (20mM Hepes pH 7.6, 1% SDS, 1X Protease Inhibitor Cocktail and 10Mm Sodium butyrate). Chromatin samples were sonicated for 14±2 cycles of 30 sec ON/30 sec OFF with the Bioruptor Pico sonication device (Diagenode) until most of the DNA fragments were 100-600 bp long (average length 200 bp). The sonicated samples were then centrifuged at ≥13000 rpm for 5 minutes at 4˚C to collect the supernatant containing the soluble chromatin fraction.

For each IP, 20µl of Dynabeads Protein A (Invitrogen, Thermo Fisher Scientific) were used. For antibody conjugation, beads were washed in ChIP dilution buffer (1% Triton x-100, 1.2 mM EDTA, 16.7mM Tris buffer pH 8, and 167mM NaCl) containing 0.01% SDS and 0.1% BSA and incubated with H3K4me3 antibody (Merk Millipore (1.5ug/IP)) in the same buffer for 1hr at room temperature with rotation. After conjugation, beads were washed, and the chromatin added; conjugated beads and chromatin were incubated in ChIP dilution buffer on a rotator for 3h at 4˚C. After incubation, beads were washed once with ChIP washing solution 1 (2mM EDTA, 20mM Tris buffer (pH 8), 1% Triton x-100, 0.1% SDS, and 150mM NaCl), twice with ChIP washing solution 2 (2mM EDTA, 20mM Tris buffer (pH 8), 1% Triton x-100, 0.1% SDS, and 500mM NaCl), and twice with ChIP washing solution 3 (1mM EDTA, 10mM Tris buffer (pH 8)). Finally, the beads were eluted in 100µl elution buffer (0.5% SDS, 300mM NaCl, 5mM EDTA, and 10mM Tris (pH 8)) containing 200µg/ml Proteinase K (Sigma-Aldrich). De-crosslinking was done by incubating samples at 55˚C for 1h followed by overnight at 65˚C. The supernatant containing the immunoprecipitated DNA was purified using Qiagen MiniElute PCR purification kit, following manufacturer instructions. Eluted DNA was used for qPCR and ChIP-seq applications. Gene promoter regions were obtained using the UCSC Genome Browser; primers were designed in house and listed in Table S3.

*ChIP-seq data analysis*

ChIP-seq libraries were prepared using the NEB NEXT Ultra II DNA-library prep kit (E7645S for ChiP and E7600S for input) and samples were sequenced on an Illumina Next-Seq to a mean depth of 38 million reads. The read length was 75pb SE. The read quality of ChIP-seq dataset was verified using fastQC (v0.11.7) with each sample showing a mean per base quality > 30 at all read positions. The data aligned to the human genome (GRCh38

version 94) using bowtie 2 (v2.3.5) with default parameters for indexing and alignment. A mean alignment of 28 million uniquely mapping reads per sample (74%) was observed. Per sample wig files were generated using the PeakRanger (1.18) wig command with format bam. Bigwigs were generated from the wig files using UCSC tools wigToBigWig (v4), with chromosome sizes as determined by UCSC tools faSize. The per sample H3K4me3 peaks were called with macs2 (v2.1.1.20160309) callpeak using the input BAM file for each sample as the control, a genome size of 2,945,849,067bp and specifying --format BAM. The alignment and peak data were inspected on the IGV genome browser (v2.7.2). Two samples (RA2 and RA4) showed high levels of noise (observable as non-peak aligned reads), low numbers of reads at peaks (10x lower than the mean) and low technical correlation with other samples. These samples were therefore excluded from the downstream analysis. Next, differential peaks between the HC and RA samples were called using the R (v3.6.2) package DiffBind (v2.14.0) using the per sample MACs broad peaks as Peaks and the per sample input BAM files as bamControl. The model was set to HC vs RA. All other parameters were left to default. DiffBind identified 6,763 significantly differential peaks at < 5% FDR from a consensus set of 75,425 peaks. The DiffBind normalised peak intensities were used for the downstream heatmap and GO analysis. The 6,763 differential peaks were annotated using Homer (v4.11.1) annotatePeaks with the databases organism human (v6.3), promoters human (v5.5) and genome hg38 (v6.4). The Gene Ontology (GO) enrichment was calculated using Homer findMotifs.pl inputting the entrez ID of the nearest TSS (within 50kb) for each peak (from the annotated peaks file) as the candidate genes. All other settings were left to default. Enriched ontologies were identified as $p < 0.0001$ and (to reduce database redundancy) a term size > 5 and < 250. The GO enrichment results are provided in supplementary dataset 1.

To identify differential peaks between responders and non-responders, firstly, responder (R) samples were identified as having a percent of inhibition > 68% (RA3, RA7

and RA11) and non-responder NR) samples as < 25% (RA1, RA6 and RA10). Next differential peaks were identified using the methods as described above however with the model R vs NR. DiffBind identified 4,172 significantly differential peaks at < 5% FDR from a consensus set of 65,717 peaks. Differential peaks were annotated, and enriched GO identified as described above. The GO enrichment results are provided in supplementary dataset 2.

*ChIP-seq visualization*

The heatmap of the 6,763 differential peaks between HC and RA (figure 5A) was generated using the R library amap (v0.8-17). Rows were clustered using the function hclust with Spearman distances and mean reordering. Diffbind normalised peak intensities were row scaled into z-scores.

To generate the network of enriched GO (figure 5C) the Homer enrichment results for biological process, molecular function and cellular component were concatenated and filtered to include only terms with an enrichment value < 0.0001 and between 5 and 250 genes with significant peaks. Each remaining ontology was considered a node and edges were drawn between two nodes where at least 50% of the genes with significant peaks were in common (Szymkiewicz-Simpson coefficient) and there were at least 5 overlapping genes with significant peaks. The network was drawn using the R package ggnet2 (v2.4) under default settings. To highlight the major functional groups, clusters with fewer than 5 nodes were removed, and representative names were given.

To generate the candidate peak (RANK, TNFR1 and TNFR2) bar-plots (Figure 5C) the promoter consensus peak (as generated previously by Diffbind) for each gene was identified using IGV. Next the read count at each peak for each H3K4me3 and input sample

was determined using the Bedtools (v2.26) multicov function. The aligned library size for each sample was determined using Samtools (v1.7) view -c with -F 260. Next the counts per million (CPM) ((count / library size) x1,000,000) at each peak was determined for each H3K4me3 and input sample. Finally, the input normalised peak intensities were calculated as: H3K4me3 CPM – Input CPM.

To create STRING networks we used the dedicated website (https://string-db.org) and the multiple proteins function under default settings[2].

*Comparison between blood CD1C and Classical Monocyte populations.*

PBMC single cell RNA-seq dataset was obtained from GEO (GSE94820) as raw counts. These were then partitioned into the pre-identified CD1C and Classical Monocyte populations and differential expression performed using DESeq2. The data was then explored with Searchlight2 using an adjusted $p < 0.01$ and absolute log2 fold change >1 and the GO biological process database. All other settings were left to default.

*RA serum analysis*

Serum from RA patients was collected by centrifugation at 1200xG for 10’ minutes, aliquoted and stored at -80˚C. Serum VEGF was evaluated using a U-PLEX Human VEGF-A (Meso Scale Diagnostics). Analysis was performed using the MSD Discovery Workbench analysis software.

*Statistical analysis*

Prism 6 (Graphpad) was used to perform all statistical analysis and statistical tests used are indicated in the figure legends. P values less than or equal to 0.05 were considered significant.



Ansalone C, *et al. Ann Rheum Dis* 2021;0:1–10. doi: 10.1136/annrheumdis-2020-219262

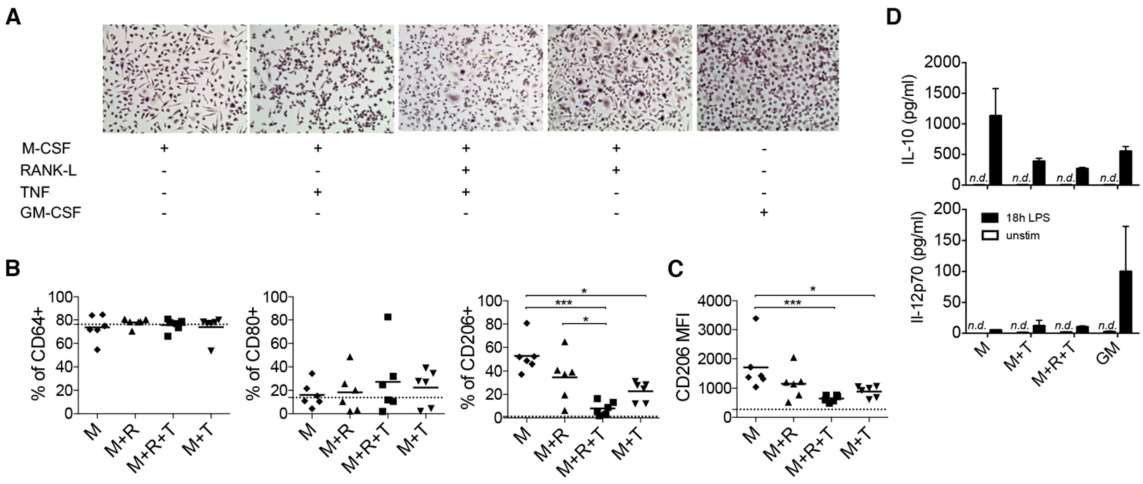


**Figure S1. TNF-driven inhibition of osteoclastogenesis does not affect apoptosis and drives CD14$^{+}$ pre-cursors toward an intermediate Mϕ phenotype.** CD14$^{+}$-derived OC pre-cursors were cultured in the presence of 25ng/ml M-CSF (M) ± 25ng/ml RANK-L (R) and ± 10ng/ml TNF (T) in various combinations. **(A)** Representative 20X magnification of TRAP-stained cultures after 3 days of cytokine stimulation. **(B)** Percentage of single cells expressing CD64, CD80, and CD206 after 72h of cytokine stimulation. **(C)** MFI of CD206 after 72h of stimulation with M, M+R, M+T, M+R+T. **(B-C)** Dotted line shows baseline at 0h of CD14$^{+}$-derived OC precursors prior R±T stimulation. Bars show mean of n=6 of two experiments pooled together. Data were analysed with Friedman test of variance and Dunn's multiple comparisons test. ***$P \leq 0.001$; *$P \leq 0.05$. **(D)** IL-10 and IL-12 release after culturing the cells for 6 days with M, M+T, M+R+T, or 100 ng/ml GM-CSF (GM). Cytokine release was measured after replacing the media with complete medium ± 100 ng/ml LPS for 18h (unstim = no LPS; n.d.=non-detectable). Graphs show mean±SD of n=3.

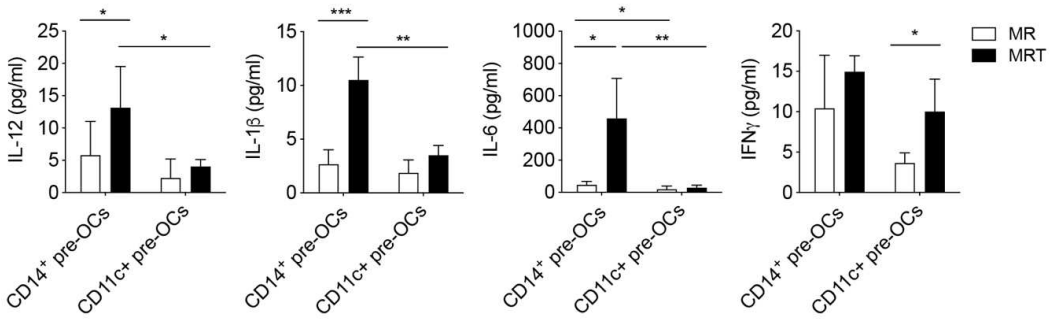


**Figure S2. CD11c$^+$ pre-OCs produces IFNγ under TNF stimulation while CD14$^+$ pre-OCs produce pro-inflammatory cytokines.** PBMCs were isolated and CD14$^+$ monocytes (MOs) and CD11c$^+$ precursors were magnetically enriched and incubated overnight with 25ng/ml M-CSF to generate CD14$^+$ and CD11c$^+$ pre-OCs, following by 72h RANK-L stimulation ± TNF (25ng/ml and 10ng/ml respectively). Cell supernatants were analysed for IL-12, IL-1β, IL-6, and IFNγ concentration. Bars show mean±SD of n=3-4. Statistical analysis was done using paired 2-way ANOVA and Sidak's multiple comparison tests.

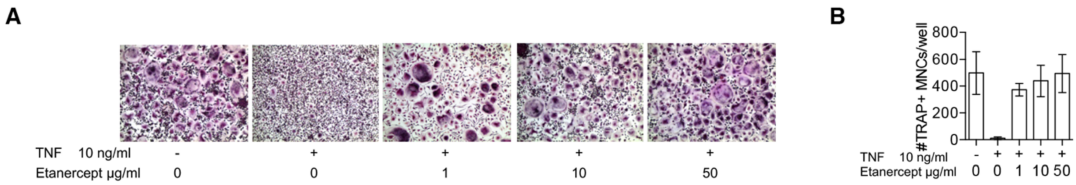


**Figure S3. Etanercept restores osteoclasts differentiation in presence of TNF.** $CD14^+$ monocytes were differentiated into OCs and OCs quantified as in Figure 1. **(A)** Representative 10X digital images of TRAP staining (purple) and **(B)** quantification of number of OCs per well after 6 days with 25 ng/ml RANK-L ± 10ng/ml TNF ± increasing concentration of etanercept (1, 10, or 50µg/ml). Bars = mean±SD (n=3). Data were analysed with two-way ANOVA and Tukey's multiple comparisons test. ****$P \leq 0.0001$.

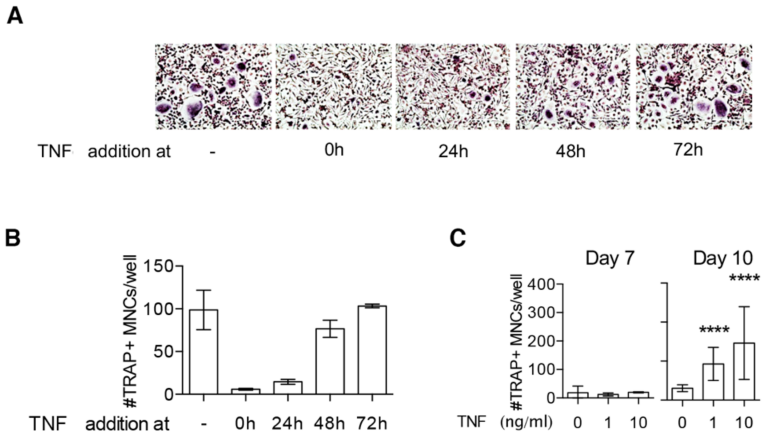


**Figure S4. TNF inhibition of osteoclast differentiation of CD14$^+$ pre-cursors is time dependant and delayed addition enhances osteoclastogenesis. (A)** Representative 20X digital images of TRAP staining and **(B)** quantification of TRAP+ MNCs/well differentiated from CD14$^+$ OC pre-cursers in the presence of 25ng/ml RANK-L for 6 days; 10ng/ml TNF was added onto the culture after 24, 48, or 72h. Error bars show mean ± SD of technical replicates of one representative experiment. The experiment was repeated twice, and similar results observed. **(C)** Quantification of TRAP+ MNCs per well after 6 days (at day 7 of the culture) or 9 days (at day 10 of the culture) of 72h of 1ng/ml RANK-L followed by additional stimulation with 1 or 10ng/ml TNF. Data were analysed using 2-way ANOVA and Dunnett's post-hoc test, comparing all data to 0 ng/ml (n=3); ****$P$<0.0001.

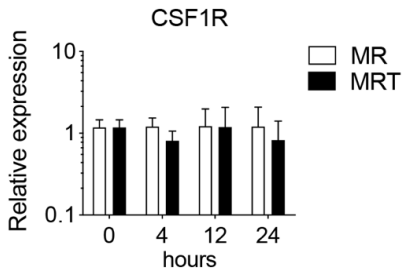


**Figure S5. TNF does not affect CSF1R expression.** Enriched $CD14^+$ monocytes (MOs) were incubated overnight with 25ng/ml to generate $CD14^+$ pre-OCs. $CD14^+$ pre-OCs were then differentiated in the presence of 25ng/ml M-CSF + 25ng/ml RANK-L (MR) or MR +10ng/ml TNF (MRT). mRNA expression of CSFR1 was evaluated at 0, 4, 12, and 24h after cytokine addition on $CD14^+$ pre-OCs. n=4.

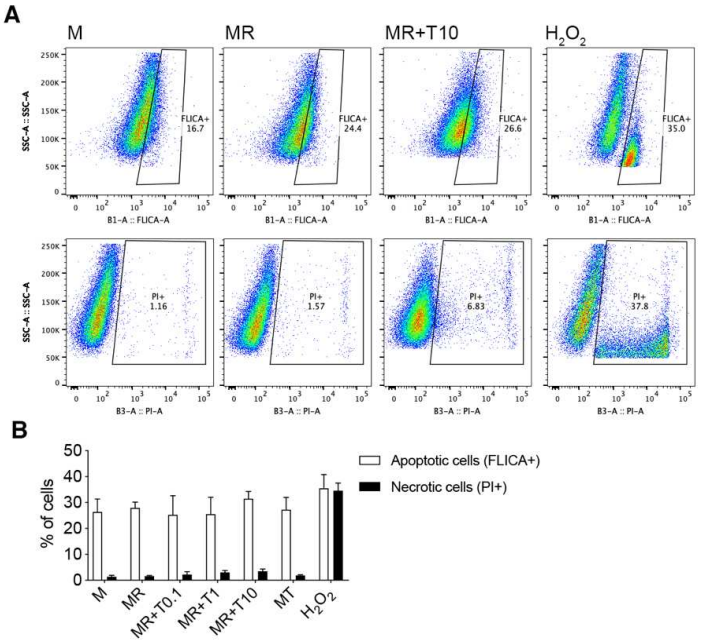


**Figure S6. TNF does not affect cell apoptosis.** CD14$^+$ monocytes were enriched from PBMCs and incubated overnight with 25 ng/ml M-CSF to obtain CD14$^+$-derived OC precursors (time 0h); these cells were subsequently incubated with 25ng/ml M-CSF ±25ng/ml RANK-L (MR) ±TNF at different concentrations (0.1, 1, or 10 ng/ml; T0.1, T1 and T10 respectively) for 48h and viability quantified using the Vybrant ® FAM Poly Caspases Assay Kit (ThermoFisher Scientific) following the manufacturer's instructions. $H_2O_2$ was used as positive control. **(A)** Representative density plots showing gating strategy for calculating apoptotic cells (FLICA +) and necrotic cells (PI+) in M-CSF (M), M±RANK-L (MR), MR±10ng/ml TNF (MR+T10), and $H_2O_2$ samples. **(B)** Quantification of % of apoptotic cells (FLICA +) and necrotic cells (PI+) in n=3 independent experiments. Error bars show mean±SD.

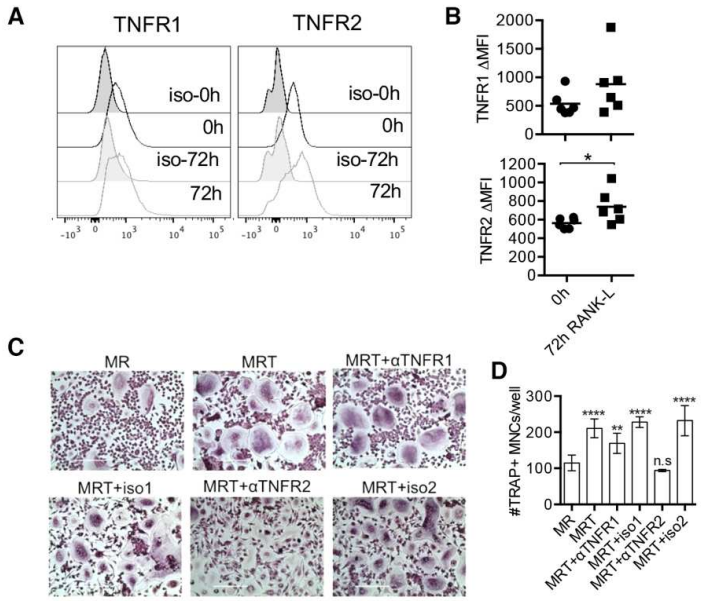


**Figure S7. TNFR2 expression increases during osteoclast differentiation and mediates TNF pro-osteoclastogenic effects in pre-fusion OCs. (A-B)** $CD14^+$ monocytes were enriched from PBMCs and incubated overnight with 25 ng/ml M-CSF to obtain $CD14^+$-derived OC precursors (time 0h); these cells were subsequently incubated with M-CSF and RANK-L (MR) for 72h to differentiate into pre-fusion OCs. **(A)** Representative half-offset histograms show TNFR1 and TNFR2 fluorescence of $CD14^+$-derived OC precursors (0h) and after 72h with 25ng/ml RANK-L (iso=isotype control for each of the TNFR antibody). **(B)** Graphs show ΔMFI of TNFR1 and TNFR2 of total single live cells at 0h and 72h of 25ng/ml RANK-L. ΔMFI of TNFR1 and TNFR2 was calculated by subtracting the MFI of the TNFR to the relative MFI of the isotype control. Data were analysed using Wilcoxon rank test for paired data. *$P \leq 0.05$. n=6 from 2 different experiments pooled together. **(C-D)** $CD14^+$-derived OC precursors were differentiated with 1ng/ml RANK-L (MR) for 72h into pre-fusion OCs and then 10ng/ml TNF was added onto the culture (MRT) ± antibody blocking TNFR1 or TNFR2 (αTNFR1 and αTNFR1) or ± the respective isotype controls (iso1 and iso2 respectively). **(C)** Representative 20X digital images of TRAP staining at day 10 **(D)**

quantification of numbers of OCs per well. Statistical significance was assessed with 2-way ANOVA and Sidak's multiple comparisons test, comparing all data to MRT. Error bars = mean±SD of n=3. ****$P$<0.0001.

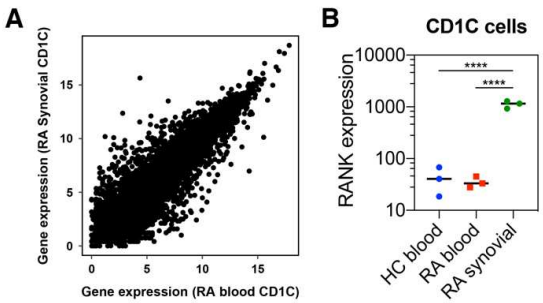


**Figure S8 - Comparison between RA blood and synovial CD1C cells.** (**A)** Comparison of global gene expression profiles between RA patient blood and synovium. Each dot is a gene. The x and y axis show expression (log10) of each gene in RA patient blood and synovium respectively. **(B)** RANK gene expression in CD1C cells isolated from HC blood, RA blood and RA synovial. Data were analysed with one-way ANOVA and Holm-Sidak's multiple comparisons test. ****=P<0.0001 and n=3.

| | |
|---|---|
| Age | 67.54±9.04 |
| Disease duration (yrs) | 11.5±8.61 |
| Seropositive | 7(12) |
| CDAI | 18.04±6.96 |
| SDAI | 24.69±13.16 |
| DAS-28(ESR) | 4.42±0.87 |
| DAS-28(CRP) | 4.14±0.82 |

**Table S1. RA patient's characteristics.** CDAI = Clinical Disease Activity Index; SDAI = Simplified Disease Activity Index; DAS = Disease Activity Score; ESR = Erythrocyte Sedimentation rate; CRP= C-reactive Protein. Values are expressed as mean±SD.

| | |
|---|---|
| RANK Forward | GCTGTAACAAATGTGAACCAGGA |
| RANK Reverse | GCCTTGCCTGTATCACAAACT |
| CFS1R Forward | TCCCAGTGATAGAGCCCAGT |
| CFS1R Reverse | CAGGGTCCAGTGAGGTGATG |
| GAPDH Forward | GAAGGACTCATGACCACAGT |
| GAPDH Reverse | GTAGAGGCAGGGATGATGTT |

**Table S2. Primer sequences used for quantitative RT-PCR.**

| | |
|---|---|
| RANK promoter Forward | GCTGGCCCCAACATTTTGAA |
| RANK promoter Reverse | CGTCGAGAATGAACGGGAGG |
| CSF1R promoter Forward | ACACTGGACACACGTTCCTC |
| CSF1R promoter Reverse | TCCAAACTCTGTGGTTGCCT |
| GAPDH promoter Reverse | TCATCCAAGCGTGTAAGGGT |
| GAPDH promoter Forward | ACTGAGATTGGCCCGATGG |

**Table S3. Primer sequences used for ChIP-PCR of promoter regions of selected genes.**

## References

1 Schmittgen TD, Livak KJ. Analyzing real-time PCR data by the comparative CT method. *Nat Protoc* 2008;**3**:1101–8. doi:10.1038/nprot.2008.73

2 Szklarczyk D, Gable AL, Lyon D, *et al.* STRING v11: Protein-protein association networks with increased coverage, supporting functional discovery in genome-wide experimental datasets. *Nucleic Acids Res* 2019;**47**:D607–13. doi:10.1093/nar/gky1131